1 **Protein features for assembly of the RNA editing helicase 2 subcomplex**
2 **(REH2C) in Trypanosome holo-editosomes**

3

4 Vikas Kumar[1#], Pawan K. Doharey[1#], Shelly Gulati[2#], Joshua Meehan[1], Mary G. Martinez[1],
5 Karrisa Hughes[2], Blaine H.M. Mooers[2*] and Jorge Cruz-Reyes[1*]

6

7 [1] Department of Biochemistry and Biophysics, Texas A&M University, College Station, Texas,
8 United States of America.

9 [2] Department of Biochemistry & Molecular Biology, University of Oklahoma Health Sciences
10 Center, Oklahoma City, Oklahoma, United States of America.

11

12 * Corresponding author:

13 e-mail: cruzrey@tamu.edu

14 * Correspondence may also be addressed to:

15 e-mail: blaine-mooers@ouhsc.edu

16

17 # These authors contributed equally to this work.

18

19

Abstract

Uridylate insertion/deletion RNA editing in *Trypanosoma brucei* is a complex system that is not found in humans, so there is interest in targeting this system for drug development. This system uses hundreds of small non-coding guide RNAs (gRNAs) to modify the mitochondrial mRNA transcriptome. This process occurs in holo-editosomes that assemble multiple mRNA *trans* factors including the RNA-free RNA editing core complex (RECC) and auxiliary RNPs. Yet, the regulatory mechanisms of editing remain obscure. The enzymatic accessory RNP complex, termed the REH2C, includes mRNA substrates and products, the multi-domain 240 kDa RNA Editing Helicase 2 (REH2) and an intriguing 8-zinc finger protein termed REH2-Associated Factor 1 (^{H2}F1). Both of these proteins are essential in editing. REH2 is a member of the DExH/RHA subfamily of RNA helicases with a conserved C-terminus that includes a regulatory OB-fold domain. In trypanosomes, ^{H2}F1 recruits REH2 to the editing apparatus, and ^{H2}F1 downregulation causes REH2 fragmentation. Our systematic mutagenesis dissected determinants in REH2 and ^{H2}F1 for the assembly of REH2C, the stability of REH2, and the RNA-mediated association of REH2C with other editing *trans* factors. We identified functional OB-fold amino acids in eukaryotic DExH/RHA helicases that are conserved in REH2 and that impact the assembly and interactions of REH2C. ^{H2}F1 upregulation stabilized REH2 *in vivo*. Mutation of the core cysteines or basic amino acids in individual zinc fingers affected the stabilizing property of ^{H2}F1 but not its interactions with other examined editing components. This result suggests that most, if not all, fingers may contribute to REH2 stabilization. Finally, a recombinant REH2 (240 kDa) established that the full-length protein is a *bona fide* RNA helicase with ATP-dependent unwinding activity. REH2 is the only DExH/RHA-type helicase in kinetoplastid holo-editosomes.

Introduction

Kinetoplastid protozoa including *Trypanosoma brucei* are early-branching eukaryotes that require extensive insertion and deletion of uridylates in most mitochondrial mRNAs (reviewed in 1). This RNA editing is protein-catalyzed and directed by small guide RNAs (gRNAs) with complementarity to fully-edited mRNA. Most editing progresses in blocks that typically overlap and each block is directed by a single gRNA (2). The editing machinery includes multiple subcomplexes: the ~20S catalytic RNA editing core complex (RECC, also called the 20S editosome) and auxiliary editing RNPs. The ~15S REH2-associated complex (REH2C) characterized here includes RNA editing helicase 2 (REH2), REH2-associated protein factor 1 (^{H2}F1), ^{H2}F2, and mRNA substrates and products (3, 4). However, only REH2 and ^{H2}F1 participate in editing. REH2C interacts with a larger accessory editing RNP complex termed the RNA editing substrate binding complex (RESC), which also contains mRNA (5, 6). The presence of mRNA in RESC was confirmed by others (7, 8).

RESC contains two modules that are intimately associated with each other: the gRNA-binding complex (GRBC) typified by the GAP1/GAP2 (alias GRBC2/GRBC1) heterotetramer that binds and stabilizes gRNA, and the more loosely defined RNA editing mediator complex (REMC) (6). REMC is typified by RGG2 and promotes editing progression (8-10). Other mRNA *trans* factors include a subcomplex containing MRB6070 and MRB1590, and RNA helicase REH1 that associate with holo-editosomes via stable or transient RNA contacts, respectively (11-13). The finding that the editing RNPs carry mRNA and gRNA implied that mRNA-gRNA hybrids form on multi-RNP platforms, and that transient addition of the RECC enzyme to the substrate-loaded platforms completes the assembly of the holo-editosome (3-8).

The editing apparatus is further complicated by the occurrence of variants of GRBC, REMC and RECC that may be regulatory (reviewed in 1) but the precise control mechanisms in editing remain unclear. However, the helicase REH2C subcomplex may play an important

71 regulatory role. REH2 is the largest characterized member of the DExH/RNA helicase A (RHA)
72 subfamily of proteins (14). These proteins are monomeric and contain a conserved C-terminal
73 domain cluster with a characteristic auxiliary oligonucleotide-binding (OB fold) domain (3, 14-
74 16). The OB fold in some RNA helicases is known to bind protein regulators or mediate RNA-
75 dependent activation of these enzymes (17). DExH/RHA proteins have a N-terminus with a
76 variable domain organization of less clear function. The N-terminal half of the REH2 carries two
77 predicted double-stranded RNA binding domains: dsRBD1 and dsRBD2 (14). Other
78 characterized DExH/RHA-type proteins that carry two N-terminal dsRBDs are the RNA helicase
79 RHA (aka DHX9) in vertebrates and its orthologous RNA helicase MLE (*maleless*) in flies (18).
80 Recombinant versions of the REH2 N-terminal half and full-size octa-zinc finger ^{H2}F1 formed a
81 stable complex *in vitro* (4). However, ^{H2}F1 is an unusual binding partner of DExH/RHA proteins
82 that typically associate with G-patch proteins (17). A genetic knockdown of ^{H2}F1 prevented
83 RNA-mediated association of REH2 with other editing components and caused fragmentation of
84 REH2 *in vivo*. Those results indicated that ^{H2}F1 is an adaptor protein and may stabilize REH2
85 (4).

86 The current study identified features in REH2 and ^{H2}F1 that affect the binding of these
87 proteins with each other, the stability of REH2, and RNA-mediated stable or transient
88 association of the REH2C subcomplex with other editing components *in vivo*. About 20 different
89 protein variants were examined *in vivo*. Comparisons of the REH2 with other eukaryotic
90 DExH/RHA helicases identified conserved OB fold residues that affect the assembly and
91 interactions of REH2C and are also important in distant processes, namely mRNA splicing in
92 yeast, and the assembly of the dosage compensation complex in fly. ^{H2}F1 upregulation
93 stabilized the large REH2 polypeptide *in vivo*. However, mutation of individual zinc fingers
94 compromised the stabilizing property of ^{H2}F1 but not its association with REH2 or other
95 examined components of the editing apparatus. Most if not all fingers may contribute to REH2

stabilization. Finally, we used a recombinant protein construct to establish that the isolated full-length REH2 (240 kDa) is a *bona fide* RNA helicase enzyme with ATP-dependent unwinding activity. REH2C is most likely an enzymatic editing RNP in kinetoplastid holo-editosomes.

Results

Previous studies revealed that the native REH2C exhibits RNA-mediated interactions with at least two variants of RESC (3-5). These variants contain gRNA and comparable levels of GAP1 and RGG2, that typify GRBC and REMC, respectively. However, these variants differ minimally in their relative content of the canonical MRB3010 in GRBC. Additional variations in protein composition have been reported in purifications of RESC components by different labs (reviewed in 1). Interestingly, native and genetically-induced changes in MRB3010 stoichiometry may be common. While the precise reasons for these changes are unclear, we reasoned that they reflect relevant dynamic changes in the assembly and function of the editing apparatus. In this study, we examined protein features that affect the formation of REH2C, its stable association with RESC components, and its transient contacts with the RECC enzyme. Because the examined helicase-associated RESC variant exhibits substoichiometric MRB3010, we refer to its variant GRBC module as GRBC* (4). Using antibodies made available to us, we have detected other proteins in pulldowns of REH2 that may be part of this RESC variant including both GAP1/GAP2 paralogs and MRB8170. The REH2 pulldowns also contain MRB6070 that was found in a MRB6070/MRB1590 subcomplex that associates via RNA with RESC (11)(S1 Fig.). However, further analysis of relative composition between variants is needed.

Analysis of REH2 mutants *in vivo*

121 We analyzed the importance of specific features of REH2, both in the formation of REH2C
122 and in the association of this subcomplex with other components in holo-editosomes (constructs
123 listed in Fig. 1A). To this end, we expressed a tetracycline (Tet)-inducible REH2 wild-type (WT)
124 construct with a Tandem Affinity Purification (TAP) tag (3) and examined its co-purification with
125 endogenous ^{H2}F1 and GAP1 proteins, of REH2C and GRBC, respectively. We found that ectopic
126 REH2 was able to reconstitute interactions of the native REH2 protein in trypanosomes (Fig. 1B-C,
127 lanes 1-2, respectively). With this system in hand, we tested the assembly of REH2 variants bearing
128 truncations or point mutations in an approach that has been used in other eukaryotic DExH/RHA
129 helicases (16, 19). All REH2 mutants examined were directly compared and normalized to a WT
130 construct used as control. Neither overexpression or depletion of REH2 affects the steady-state
131 level of its binding partner ^{H2}F1 or the examined GRBC proteins (3, 4).
132
133 **Fig. 1. *In vivo* analyses of REH2 variants. (A)** Scheme of REH2 WT (2167 residues) and
134 variants with the examined truncations or point mutations in the N- and C-terminal regions (NTR
135 and CTR). The mutations, affected domains, and predicted molecular weight of the constructs
136 are listed. Identified domains: dsRBD1 and dsRBD2 (double-stranded RNA binding domains 1
137 and 2), CORE (catalytic core RecA1 and RecA2 domains), HA2 (helicase associated helical
138 bundle domain), and OB (OB fold-like domain). **(B-C)** Western blots of IgG pulldowns from
139 extracts to examine the association of tagged REH2 WT or deletion mutants with endogenous
140 ^{H2}F1 and GAP1. An uninduced (-Tet) control lane is included. The data are representative of at
141 least three biological replicates for each mutant. A few non-specific species cross-react with the
142 antibodies in some assays. The position of IgG is marked. Sizing markers (M) are in kDa. **(D)**
143 Charts of the relative level of ^{H2}F1 and GAP1 in the pulldowns. Representative assays from
144 panels A-B and other pulldowns in this study were used to plot +/-1 SD, *n*=3 for each mutant.
145 The ^{H2}F1/REH2 and GAP1/REH2 ratios in each REH2 mutant were normalized to the ratios in
146 REH2 WT (= 1, in the plot). Assays with signals that were too low were not determined (n.d.).

147 REH2 was often fragmented, so only the full-length polypeptide was scored. Some short
148 deletion mutants were present at higher level than tagged REH2 WT in the induced extracts.
149
150 *N- and C-truncations*. We examined N- and C-terminal regions (NTR and CTR) flanking the
151 catalytic and helicase associated domains RecA1/RecA2 and HA2, respectively, in REH2. We
152 removed sequences in the unique NTR (>1000 residues) in the REH2 variants ΔN and ΔNds. Next,
153 we removed the CTR after the OB fold (123 residues) or from the OB fold (260 residues) in the ΔAOB
154 and ΔOB variants, respectively. REH2 and its orthologs in kinetoplastids carry the longest N terminus
155 in the known DExH/RHA-type helicases (~1300 residues in REH2 from *T. brucei*) (14). Direct
156 comparisons with the REH2 WT construct showed that the examined N- and C-resections reduced
157 the association of the shortened REH2 polypeptides with ^{H2}F1 and GAP1 proteins (Figs. 1B-D). This
158 suggested that both termini of REH2 may contribute to the normal assembly of REH2C and its RNA-
159 mediated interactions with other editing components *in vivo*. The dsRBDs, the OB fold, and
160 undefined features in the N and C termini may be involved. It is also conceivable that the examined
161 sequence resections may impact the global conformation of REH2, thereby indirectly affecting its
162 protein interactions. In that case, the normal REH2 interactions in the editing apparatus may be
163 sensitive to overall changes in the integrity or conformation of REH2. A comparison of REH2 ΔN and
164 ΔNds in whole-cell and enriched-mitochondrial extracts indicated that these large truncations do not
165 prevent mitochondrial import (S2 Fig). Because the CTR includes a potentially regulatory OB fold in
166 DExH/RHA-type RNA helicases (16), we focused on this domain in the subsequent studies of REH2.
167
168 *Point mutations*. Our structural searches of the OB fold-like domain in REH2 using Phyre2
169 (20) found the best agreements of the REH2 OB fold with structures of yeast ADP-bound Prp43p
170 helicase and *Drosophila* RNA helicase MLE in a complex with RNA and ADP-Alf4 (4, 16, 18, 21).
171 Prp43p is a bi-functional helicase in mRNA splicing and ribosome biogenesis (15, 22). The helicase

172 MLE remodels roX RNA substrates to promote assembly of the dosage compensation complex in
173 *Drosophila* (18). We examined specific residues in the predicted OB fold of REH2 that seem to be
174 conserved in the DExH/RHA helicases mentioned above (Fig. 2 A-D). OB point mutations were
175 compared to two controls: REH2 WT and a mutation in dsRBD2 (dsR) that reduces the association of
176 REH2 with GAP1, gRNA and mRNA (Fig. 2A, lanes 1 and 2, respectively) (3). The $\beta1-\beta2$ and $\beta4-\beta5$
177 loops in the OB fold may include determinants in nucleic acid recognition (Fig. 2D) (16, 18). In
178 helicase Prp43p, mutation of K704, which is exposed to the solvent in the Prp43p structure,
179 decreased the RNA affinity and ATPase activity of the helicase *in vitro* (16). Sequence alignments
180 and a homology model derived from the structure of Prp43p matched K704 in Prp43p with R2023 in
181 the predicted $\beta4-\beta5$ loop in REH2 (S3 Fig)(4). We also examined R1979 in REH2 that is not
182 conserved in Prp43p and may serve as an internal control. Pulldowns of the R1979A and R2023A
183 mutants suggest that neither mutation alters the association of REH2 with ^{H2}F1 (Figs. 2A-C). R1979A
184 did not appear to affect the REH2 association with GAP1. However, R2023A caused a moderate
185 decrease in the association with GAP1, implying that at least R2023A could be disruptive in
186 trypanosomes.

187 In helicase MLE, several residues in the OB fold bind to specific uridylates in U-rich
188 sequences in roX transcripts. Mutation of some of these residues impaired RNA binding by MLE *in*
189 *vitro* or the proper localization of MLE in chromosomes (18). Sequence alignments and homology
190 models indicated that the residues H1032 and K1033 in MLE likely represent residues H1998 and
191 R1999 in the predicted $\beta3-\beta4$ loop in the OB fold in REH2 (Fig. 2D; S4 Fig)(21). The H1998E mutant
192 appeared to retain a normal association with ^{H2}F1 but exhibited a moderate decrease in association
193 with GAP1. In contrast, R1999E either alone or together with H1998E (98/99) exhibited a more
194 robust decrease (over 60%) in association with both ^{H2}F1 and GAP1 (Fig. 2A-C). This indicated that
195 H1998 and R1999 contribute to the assembly of the REH2 helicase with other editing components.
196 However, R1999 has a higher impact on such interactions than the adjoining H1998. As expected,

197 the dsR mutant used as a control exhibited a strong decrease in association with GAP1. However,
198 the dsR mutation did not seem to affect the association of REH2 with ^{H2}F1 (Figs. 2A, 2C). Pulldowns
199 of the mutants were normalized to the REH2 WT control as in Fig. 1.
200
201 **Fig. 2. *In vivo* analyses of REH2 variants.** Western blots of IgG pulldowns as in Fig. 1 to
202 examine the association of endogenous ^{H2}F1 and GAP1-associated complexes with tagged
203 REH2 WT or variants with point mutations in the OB fold domain at: **(A)** R1979A (1979),
204 H1998E (1998) and R1999E (1999); and **(B)** double 1998/1999 (98/99) or single mutation at
205 2023. The previously characterized dsR mutant with an inactivating double mutation in the
206 dsRBD2 was included for comparison in panel A (3). A few non-specific species crossreact with
207 the antibodies in some assays. **(C)** Charts of the relative levels of ^{H2}F1 and GAP1 in the
208 pulldowns. Assays from panels A-B and biological replicate pulldowns in this study were used to
209 plot +/-1 SD, *n*=2 or *n*=3 for each mutant. The ^{H2}F1/REH2 and GAP1/REH2 ratios in each REH2
210 mutant were normalized to the ratios in REH2 WT (= 1, in the plot). **(D)** Secondary structure
211 prediction of the OB fold with α-helix (cylinders) and β-strand (arrows) elements, and the
212 position of point mutations examined indicated by arrows.
213
214 Table 1 summarizes observed effects of the examined mutations in REH2 on its association
215 with ^{H2}F1 and GAP1. While large protein truncations in REH2 may alter the global conformation of
216 the polypeptide, relevant point mutations in REH2 are more likely to cause specific functional effects.
217 Our systematic mutagenesis of REH2 suggests an intricate interaction network including features
218 across both N- and C- terminal regions of REH2 that affect the assembly of REH2C, and the
219 association of this subcomplex with other components of the editing apparatus *in vivo*. Remarkably,
220 these observations also indicate that equivalent residues in the auxiliary conserved OB fold domain
221 in DExH/RHA helicases function in disparate RNA processes in the taxonomically distant species of
222 trypanosomes, yeast, and fly.

223 **Table 1. Association of REH2 constructs with ^{H2}F1 and GAP1**

REH2-TAP variant	Association in pulldown		Reference
	^{H2}F1	GAP1	Construct described
WT	control*	control*	23
ΔN	decreased	decreased	This study
ΔNds	decreased	decreased	This study
ΔOB	decreased	decreased	This study
ΔAOB	decreased	decreased	This study
dsR	control-like †	decreased	3
1979	control-like	control-like	This study
1998	control-like	decreased	This study
1999	decreased	decreased	This study
98/99	decreased	decreased	This study
2023	control-like	decreased	This study

* The WT construct served as positive control to assess relative association of mutant constructs.

224 † Comparable to the level observed with the WT construct.

225

226 ## Analysis of ^{H2}F1 mutants *in vivo*

227

228 To analyze specific features of the ^{H2}F1 zinc finger protein in trypanosomes, we expressed a
229 Tet-inducible tagged ^{H2}F1 WT construct and examined its association with endogenous REH2, GAP1
230 and REL1 proteins. REL1 is a subunit of the editing enzyme RECC. We found that the tagged ^{H2}F1
231 WT was able to reconstitute interactions of the native ^{H2}F1 protein in trypanosomes (Fig. 3). Notably,
232 expression of the ectopic ^{H2}F1 WT increased the steady-state level of endogenous REH2 compared
233 to a control lane without tetracycline (Fig. 3A, lanes 1-2; Fig. 3B). As a control to mark the position of
234 REH2 we used a reported RNAi-based knockdown of ^{H2}F1 that decreases the level of endogenous
235 REH2 (Fig. 3A, lanes 5-7; Fig. 3B)(4). The contrasting effects of the upregulation and downregulation
236 of ^{H2}F1 on the endogenous REH2 are consistent with the idea that ^{H2}F1 stabilizes REH2 *in vivo*. We
237 examined the distribution of REH2 and ^{H2}F1, and canonical proteins in RESC and RECC, in
238 sedimentation analyses of mitochondrial extract (S5 Fig). REH2 is heterodispersed as shown before
239 (23) and overlaps with ^{H2}F1 in the gradient. However, the relative abundance of these proteins at
240 high and low densities differs substantially. It is possible that the association between REH2 and ^{H2}F1

241 or their stoichiometry in REH2C varies *in vivo*. Additional studies will be necessary to examine these
242 possibilities.
243
244 **Fig 3. Effect of expressing ^{H2}F1 WT or Zn5 C2>A2 on the REH2 steady state abundance.**
245 Figure annotations use short acronyms for each mutant in the form: Z*X*. **(A)** Western blots of
246 extracts with tagged ^{H2}F1 WT (lanes 1-2) or Z5 C2>A2 (Z5; lanes 3-4). Control assays include
247 lanes without Tet-induction. Control lanes with a reported ^{H2}F1-RNAi construct mark the position
248 of the endogenous REH2 and ^{H2}F1. The RNAi lanes show the induced decrease of ^{H2}F1 and
249 concurrent fragmentation of REH2 full-length. Hash marks indicate full-length and two prominent
250 fragments of REH2 (4). GAP1 was used as a loading control in all assays in this panel.
251 Molecular size markers (M). A typical C2H2 zinc finger domain fold is depicted with core
252 cysteine substitutions C2>A2 (arrows), other conserved residues, and variable residues (black
253 circles). **(B)** Charts of the relative levels of endogenous REH2 full-length in the extracts +/-1 SD,
254 *n*=3. Induced/uninduced ratios of REH2 for each construct were further normalized to GAP1. **(C-**
255 **D)** IgG pulldowns of WT and Z5 constructs showing association with endogenous REH2, GAP1,
256 REL1, and endogenous ^{H2}F1. REL1 is examined by radiolabeled self-adenylation. Other
257 proteins are examined as in panel A. Non-specific species (*) may represent fragments of the
258 tagged protein that react with the antibodies. **(E)** Charts of the relative levels of REH2, GAP1
259 and REL1 in the pulldowns +/-1 SD, *n*=3. The ratios (protein/tagged-bait) in the Z5 mutant were
260 normalized to ratios in the ^{H2}F1 WT construct.

261
262 To determine if the stabilizing effect of ^{H2}F1 requires one or more zinc finger (Znf) domains,
263 we introduced amino acid substitutions that either disrupt the canonical fold of the domain (by
264 replacing the canonical residues) or eliminate the positive charge (by replacing various basic
265 residues with neutral residues) in individual fingers of the ectopic construct. The examined ^{H2}F1
266 mutants are summarized in Table 2. The location of the fingers and the examined substitutions

267 (between 2 and 5 per finger) in the full sequence of ^{H2}F1 are shown in S6 Fig. All ^{H2}F1 mutants
268 examined were directly compared and normalized to a WT construct used as control in all
269 panels. This enabled the separation of mutants in multiple panels.

270 **Table 2. ^{H2}F1 mutants with reduced ability to stabilize REH2 *in vivo***

^{H2}F1-TAP variant	Endogenous REH2 *Steady-state level*	Figures using this construct
WT	**Increased***	Figs. 3, 4 and 5
Znf5 C2>A2	no change †	Fig. 3
Znf1 R/K>A	no change	Fig. 4
Znf2 R/K>A	no change	Fig. 4
Znf3 R/K>A	no change	Fig. 4
Znf4 R/K>A	no change	Fig. 5
Znf5 R/K>A	no change	Fig. 4
ΔN	no change	Fig. 5
ΔC	no change	Fig. 5

* ^{H2}F1-WT ectopic expression increased the level of endogenous REH2
271 † No change (i.e., level within stardard deviation for at least two biological replicates)
272
273 *Canonical cysteine residues*. We changed two cysteines to two alanines (C2>A2) to disrupt
274 the native conformation of the predicted zinc fingers (Fig. 3A). We began by disrupting Znf5 because
275 of its significant homology to a reported dsRNA-bound C2H2 zinc finger domain structure (4, 14, 24).
276 Mutants are referred to in the text by the acronym in the general form Znf*X*. A shorter version of the
277 acronym is used in the figure annotations. The resulting mutant protein Znf5 C2>A2 did not induce an
278 evident increase in the steady-state level of endogenous REH2 as we found after expressing the
279 ^{H2}F1 WT construct. This was evident in direct comparisons of extracts that contain similar levels of
280 ectopic ^{H2}F1 protein, WT or Znf5 C2>A2 (Fig. 3A, lanes 1-4; Fig. 3B). To examine whether the lack of
281 Znf5 affected the association of ^{H2}F1 with other editing components, we performed IgG pulldown
282 assays of tagged ^{H2}F1. These assays showed that the ^{H2}F1 WT and Znf5 C2>A2 variants similarly
283 associated with endogenous helicase REH2, GAP1 and REL1 ligase (Figs. 3C, 3E). Notably,
284 pulldowns of both tagged ^{H2}F1 WT and Znf5 C2>A2, contain endogenous ^{H2}F1 (Fig. 3D). The above

285 data suggest that Znf5 is not essential for the normal association of ^{H2}F1 with other editing
286 components.
287 We also attempted to generate a ^{H2}F1 variant bearing a triple C2>A2 substitution in Znf6,
288 Znf7 and Znf8. However, expression of this construct was unstable and eventually lost in culture.
289 Together, the observations above suggest that ^{H2}F1 may require a full complement of zinc fingers in
290 their native conformation to stabilize REH2 but not to associate with the examined editing
291 components.
292
293 *Variable basic residues*. Because the native conformation of the zinc fingers seems to be
294 required for ^{H2}F1 to stabilize REH2 we introduced mutations that decrease the positive charge in the
295 zinc fingers yet likely to retain native conformation (25). We expressed ^{H2}F1 variants to test the role
296 of several basic residues around the core residues that are mostly located between the second
297 cysteine and the first histidine (Fig. 4A) (26). Specifically, we introduced R/K>A substitutions
298 (between 2 and 6 per finger) to decrease the positive charge in the zinc fingers and to remove
299 potential charge-charge interactions with REH2 or associated RNAs. As above, we use in the text the
300 acronym in the general form Znf*X* but a shorter version of the acronym in the figures. Our functional
301 analyses of Znf1, Znf2, Znf3 or Zn5 R/K>A variants showed that the loss of positive charge in any of
302 these zinc fingers reduced the ability of ^{H2}F1 to induce the accumulation of intact endogenous REH2
303 in extracts (Figs. 4B-C). However, these mutations did not prevent the association of ^{H2}F1 with
304 REH2, GAP1 and REL1 (Figs. 4D-F). These expressed ^{H2}F1 variants also co-purified with
305 endogenous ^{H2}F1 at a level comparable to the WT construct (Figs. 4D, 4F). The data above indicated
306 that the wildtype and R/K>A variant proteins associated similarly with the examined editing
307 components. Overall, ^{H2}F1 may require that most zinc fingers retain their native conformation and
308 positive charge to efficiently increase the stability of REH2. However, the loss of the native
309 conformation or positive charge in individual fingers does not preclude the assembly of ^{H2}F1 in the
310 REH2C, or the association of this subcomplex with the examined editing components. Detection of

311 endogenous ^{H2}F1 in our pulldowns suggest the presence of ^{H2}F1 multimers. Pulldowns treated with
312 an RNaseA/T1 mixture suggest that the association between tagged ^{H2}F1 and endogenous ^{H2}F1 is
313 RNase-resistant (S7 Fig.). However, further studies using isolated recombinant proteins are needed
314 to establish direct protein contacts between ^{H2}F1 monomers as was shown between REH2 and ^{H2}F1
315 (4).
316
317 **Fig. 4. *In vivo* analyses of ^{H2}F1 variants with reduced positive charge in Znf1, Znf2, Znf3**
318 **or Znf5 (variable residues R/K>A).** Figure annotations use a shorter acronym of the mutant in
319 the form: Z*X*. **(A)** Cartoon of ^{H2}F1 (524 residues). Multi-sequence alignment of the eight C2H2
320 zinc fingers, indicating the core cysteines and histidines (boxes) and R/K>A substitutions of
321 variable residues (between 2 and 6) in each finger (open circles). The C2H2 zinc finger domain
322 fold is depicted as in Fig. 3. In this case, the arrows illustrate three variable residue substitutions
323 R/K>A. **(B)** Western blots of extracts as in Fig. 3A of induced tagged ^{H2}F1 WT and Z1, Z2, Z3
324 and Z5 R/K>A mutants or uninduced control. GAP1 was used as a loading control (lanes 1-7).
325 **(C)** Chart of steady-state level of endogenous REH2 full-length in extracts with each construct
326 as in Fig. 3B. **(D-E)** Western blots and self-adenylation reactions of IgG pulldowns of ^{H2}F1 WT
327 and Z1, Z2, Z3 and Z5 R/K>A mutants showing association with endogenous REH2, ^{H2}F1,
328 REL1 and GAP1. Non-specific species in pulldowns (*) are indicated. (**F)** Charts of the relative
329 levels of associated endogenous proteins in the pulldowns +/-1 SD, *n=2* or *n*=3, as in Fig. 3.
330 The ratios (protein/tagged-bait) in the mutants were normalized to ratios in the ^{H2}F1 WT
331 construct.
332
333 *N- and C-truncations*. Because mutagenesis of the tested Znf domains did not prevent the
334 association of ^{H2}F1 with other editing components *in vivo*, we asked if fragments of ^{H2}F1 retain these
335 interactions. To test this question, we expressed N- or C-terminal fragments including Znf1-to-Znf3
336 (termed ΔC) or Znf4-to-Znf8 (termed ΔN) that span 49% and 51% of the ^{H2}F1 polypeptide chain,

337 respectively (Fig. 5A, bottom). These two fragments exhibited minimal or no association with the
338 examined endogenous REH2, ^{H2}F1, or REL1 ligase (Figs. 5A). These mutants were directly
339 compared with the ^{H2}F1 WT and Znf4 R/K>A constructs. We note that while Znf4 R/K>A was
340 examined separately from the R/K>A variants in Fig. 4, all R/K>A mutants are normalized to the ^{H2}F1
341 WT construct that was included in all gels. The Znf4 R/K>A and other Znf R/K>A mutations in the
342 current study retained all tested interactions that are observed with the ^{H2}F1 WT control. However,
343 the ΔN and ΔC constructs failed to establish basic interactions with the tested editing components.
344 Because the native REH2C subcomplex carries mRNA (4), we wondered if the ^{H2}F1 ΔN and ΔC
345 constructs also fail to co-purify with mRNA. To this end, we quantitated the relative content of
346 mitochondrial transcripts in the pulldowns of the WT, ΔN, and ΔC constructs in biological replicate
347 experiments that were performed in triplicate (Fig. 5B). The examined mitochondrial transcripts
348 include examples of unedited, edited, and never-edited mRNA, the never-edited mRNA ND4, and
349 ribosomal RNA 9S. We also examined cytosolic transcripts (Tubulin, 1400 and 1390) to score non-
350 specific RNA interactions of editing subcomplexes as in previous pulldown studies (5). Relative to the
351 ^{H2}F1 WT control used for normalization, both ΔN and ΔC pulldowns exhibited a dramatic loss in
352 bound mitochondrial mRNAs (Fig. 5B, upper and middle panels). Interestingly, the levels of cytosolic
353 mRNAs were similar in the ΔN and WT proteins but dramatically less in the ΔC variant. The later
354 variant lost most examined RNA interactions: specific and non-specific. An exception may be
355 mitochondrial RNA 9S. We also compared the relative impact of the ΔN and ΔC deletions with a
356 more discrete alteration in Znf4 R/K>A (Fig. 5B, lower panel). The level of mitochondrial RNAs in the
357 Znf4 pulldown was similar to that of the ^{H2}F1 WT control. However, the level of cytosolic transcripts
358 decreased ~70 fold in Znf4 R/K>Ala. The independent pulldowns and RNA quantitation in three
359 equivalent experiments showed consistent results in the protein interactions and RNA content of
360 these ^{H2}F1 constructs. The above data indicated that the tested ^{H2}F1 fragments appear to have lost
361 the normal direct interaction of ^{H2}F1 WT with REH2 in REH2C, and the normal RNA-dependent

362 association of ^{H2}F1 WT with other examined proteins in the editing apparatus. Quantitation of the
363 examined transcripts in the input extracts (including those used in the pulldowns in Figs. 5A-B)
364 confirmed that the observed dramatic loss in RNA association with ΔN and ΔC constructs was not
365 due to large changes in the transcripts level at steady state (S8 Fig.). The above observations
366 indicate that features in both termini of ^{H2}F1 are required for efficient association of mitochondrial
367 transcripts in the pulldowns of ^{H2}F1. The ^{H2}F1 ΔN construct used a heterologous mitochondrial leader
368 sequence (see methods and S1Table). A comparison of ^{H2}F1 ΔN and ΔC in whole-cell and enriched-
369 mitochondrial extracts suggest that ^{H2}F1 ΔN localizes to mitochondria efficiently. However, the import
370 or retention of ^{H2}F1 ΔC into mitochondria may be relatively compromised. At least some import of the
371 ^{H2}F1 ΔC construct may occur in comparison with a control cytosolic marker (S2 Fig.). Finally, the
372 more discrete alteration in Znf4 R/K>A may have caused a relatively mild decrease in RNA affinity
373 that mostly affected weak, non-specific interactions, e.g., by cytosolic RNA in the pulldowns of ^{H2}F1.
374

375 **Figure 5. *In vivo* analyses of ^{H2}F1 terminal deletion and Znf4 mutants. (A)** IgG pulldowns of
376 N and C truncation mutants (ΔN and ΔC) that removed fingers 1-to-3 and fingers 4-to-8,
377 respectively, and the Z4 R/K>A variant. Association of the constructs with endogenous REH2,
378 ^{H2}F1 and REL1 was examined. Biological replicates of these assays suggest a similar quality
379 and loading of samples in the pulldowns. Cartoon of ^{H2}F1 with zinc fingers and a line marking
380 the N and C truncations. **(B)** qRT-PCR quantitation of transcripts in the pulldowns in panel A.
381 dCq of IgG pulldowns of tagged protein (induced extract) normalized to a mock pulldown
382 (uninduced extract) [dCq = $2^{(\text{test Cq} - \text{mock Cq})}$] for each construct. The mutant proteins were then
383 normalized to the tagged WT protein. All values took into account the recovery of tagged protein
384 in each pulldown in panel A. Three independent biological replicates with Cq average values
385 and one standard deviation (+/-1 SD, *n*=3) were plotted. Non-specifically associated cytosolic
386 transcripts differed substantially in pulldowns of different mutants, so these transcripts were not

387 used as reference. Mitochondrial unedited (UE) and edited (ED) and cytosolic RNA transcripts
388 are indicated. RPS, Murf, and 9S are abbreviations for RPS12, Murf2 and 9S rRNA. 1390 and
389 1400 are abbreviations for the cytosolic HGPRT isoforms Tb927.10.1390 and Tb927.10.1400,
390 respectively. Tub is tubulin. Other short names are standard.
391

392 **Analysis of recombinant REH2 *in vitro***
393
394 The conserved predicted catalytic domains in REH2, the unwinding activity of pulldowns of
395 REH2 and ^{H2}F1 from extracts, and the loss of this activity in the pulldowns due to mutation of catalytic
396 amino acids in REH2 indicate that REH2 in the context of its native subcomplex in trypanosomes
397 functions as an RNA helicase (3, 4, 23). However, the unwinding activity of the isolated REH2 has
398 not been formally established. We have now generated a his-tagged recombinant full-length rREH2
399 polypeptide (240 kDa) without its mitochondrial leader sequence (see the methods section) that
400 supports robust ATP-dependent unwinding of a synthetic dsRNA substrate *in vitro.* This polypeptide
401 is largely intact in most preparations (Fig. 6A). The dsRNA substrate in our assay is a mimic of the
402 native A6 editing system formed by pre-annealing of a 3' fragment of the pre-mRNA A6 with a
403 cognate gRNA. The synthetic A6 mRNA/gRNA pair supports a full round of U-deletion editing in
404 an *in vitro* assay with cell extracts and purified RECC enzyme (27, 28). The unwinding activity of
405 the recombinant enzyme increased in a titration with increasing concentrations of rREH2, and also in
406 a time course up to 30 min when most of the annealed radiolabeled RNA was unwound (Figs. 6B-C).
407 An upshift of radiolabeled RNA in a ribonucleoprotein complex at the highest tested concentrations of
408 rREH2 in the titration may be due to the known RNA binding activity of the native REH2 established
409 by UV crosslinking (5, 23). The radiolabeled strand alone (gRNA) and in heat-treated controls of the
410 dsRNA substrate exhibit the same gel mobility as the helicase-unwound gRNA (Figs. 6C-D). In
411 summary, the isolated 240 kDa recombinant REH2 is a *bona fide* RNA helicase enzyme *in vitro*, and
412 further supports the idea that REH2 may remodel RNA or its RNPs in editing.

413

414 **Figure 6. Recombinant rREH2 is a catalytically active RNA helicase. (A)** Purified rREH2[30-
415 2167] samples in a denaturing gel stained with Coomassie. NTA-Ni elution fractions 1-to-3 are
416 shown with molecular size markers (kDa). **(B)** Unwinding assays in 10 μL reaction mixtures with
417 increasing concentrations of rREH2[30-2167] +/- ATP. A ribonucleoprotein complex (RNP)
418 forms at the highest enzyme concentration tested; **(C)** Unwinding assays at increasing
419 incubation times with rREH2[30-2167] +/- ATP using the standard reaction mixture described in
420 the material and methods section. The standard reaction used a molar excess of enzyme over
421 substrate. The dsRNA (ds) was assembled by pre-annealing of synthetic transcript that mimics
422 a 3' fragment of the *T. brucei* A6 pre-edited mRNA and a radiolabeled cognate guide RNA (27).
423 Radiolabeled unwound ssRNA (ss) is indicated. Input dsRNA was heat denatured (Δ) as control.
424 **(D)** Additional controls showing that the starting radiolabeled ssRNA used to generate the
425 dsRNA substrate in the assay and the unwound radiolabeled ssRNA in the heat-denatured (Δ)
426 dsRNA (in panel B) have the same gel mobility.

427

428 # Discussion

429
430 In the current study, we examined over 20 constructs of REH2 and ^{H2}F1 (Tables 1 and 2) to
431 identify features in these editing proteins that impact the stability of REH2, the assembly of the
432 REH2C RNP, and its RNA-mediated coupling with other components of the RNA editing holoenzyme
433 (or RNA holo-editosome). We also formally established that the isolated REH2 is a bona fide RNA
434 helicase enzyme.

435

436 The mRNA editing *trans* factors core enzyme RECC and accessory RESC and REH2C
437 exhibit transient and stable contacts with each other via RNA. Variants of RECC and the RESC

438 modules, GRBC and REMC, are also emerging in studies by different labs (reviewed in 1). These
439 variants imply a dynamic nature of holo-editosomes that may be important in editing control and
440 needs further characterization. The helicase complex REH2C exhibits transient and stable contacts
441 with variants of RESC that minimally differ in the relative content of MRB3010 (in the GRBC module).
442 This study focused on stable interactions by REH2C that can be readily examined. Prior studies *in*
443 *vivo* showed that inactivating mutations in the helicase ATP binding site or the dsRBD2 domain
444 dissociate REH2 from mRNA and RESC components, suggesting a general helicase detachment
445 from the editing apparatus (3). ^{H2}F1 RNAi dissociates the helicase from canonical proteins in the
446 RESC modules. RNAi knockdown of either ^{H2}F1 or REH2 also inhibited the editing associated with a
447 RESC variant that is particularly active and transiently interacts with REH2C (3, 4). These and other
448 observations indicate that transient and stable contacts in dynamic holo-editosomes including
449 those involving REH2C are important.
450 A systematic mutagenesis in the current study identified features affecting the assembly of the
451 REH2C RNP, or its association with other editing components *in vivo.*
452

453 **REH2 mutants *in vivo***
454
455 The NTR truncations examined here (>1000 residues each), ΔN and ΔNds, caused a major
456 loss in ^{H2}F1 binding and RNA-mediated association with GAP1. The only difference between the ΔN
457 and ΔNds constructs is that the latter lacks the ~70 amino acid dsRBD2 domain. As mentioned
458 above, the dsRBD2 promotes the addition of REH2 into holo-editosomes (3). Also, the dsRBD2 in the
459 related helicase MLE in flies may provide a major RNA-binding surface (29, 30). The tested
460 truncations suggest that other N-terminal features besides dsRBD2, may contribute to normal
461 interactions by REH2 *in vivo*. These truncations may also introduce topological changes that alter the
462 normal REH2 interactions but did not prevent localization of the constructs in enriched-mitochondrial
463 extracts (S2 Fig.). Conformational changes were proposed to modulate interactions by other

464 eukayotic DExH/RHA helicases (18, 31). Overall, the tested NTR truncations may indicate the
465 presence of unidentified protein features or global changes in conformation that affect the REH2
466 interactions. Further studies will be needed to resolve these possibilities. However, relatively short
467 CTR truncations and point mutations that affected the REH2 interactions with other editing
468 components are less likely to cause major conformation changes in REH2.
469
470 We have speculated that the conserved OB fold in DExH/RHA subfamily helicases may
471 share functional residues in kinetoplastid RNA editing and other RNA processes (14). Our examined
472 C-terminal truncations included most of the CTR (260 residues in ΔOB) or elements beyond the
473 OB fold that may be specific of REH2 (123 residues in ΔAOB). We examined R2023 in REH2
474 that corresponds to R704 in helicase Prp43p in yeast spliceosomes (16) (S3 Fig.). R2023
475 should be located in a critical loop, β4-β5, in the REH2 OB fold. In yeast, R704 is poised to
476 interact with the RNA substrate entering the helicase cavity, and mutation of this residue inhibits
477 the RNA binding and RNA-mediated activation of Prp43p (16). We also examined R1979 in
478 REH2, which is not conserved in Prp43p. In trypanosomes, the R2023A substitution had a
479 moderate effect on the stable RNA-mediated association of REH2C with GAP1. However,
480 R1979A did not evidently affect this interaction. Neither R1979A or R2023A seem to
481 significantly affect the REH2 direct interaction with ^{H2}F1.
482 Similarly, H1998 and R1999 in REH2 were compared to the equivalent H1032 and
483 K1033 positions in the RNA helicase MLE in flies. The later residues in MLE bind specific
484 uridylates in U-rich roX boxes of the cognate roX RNA. H1032 and K1033 are also needed for
485 the chromosomal localization of MLE in the *Drosophila* dosage compensation complex (18). The
486 H1998E substitution had a moderate effect on the REH2 association with GAP1 but had little or
487 no effect on the interaction with ^{H2}F1. In contrast, the adjacent substitution R1999E affected
488 both the direct REH2 interaction with ^{H2}F1 and the RNA-based REH2 association with GAP1.

489 These results are consistent with the idea that ^{H2}F1 is an adaptor protein of REH2 (4), and that
490 structure-function correlations may be tractable to specific conserved amino acids in REH2 and
491 related helicases in highly-diverged species (14). This is also in line with the idea that the OB
492 fold in DExH/RHA helicases, including REH2, is a conserved regulatory domain.
493

494 **^{H2}F1 mutants *in vivo***
495
496 ^{H2}F1 has eight predicted C2H2 Znf domains that cover over ~45% of the polypeptide
497 sequence. Apart from the Znf domains, ^{H2}F1 has no evident sequence or structural conservation
498 outside of the kinetoplastids. Besides serving as an adaptor protein (4) ^{H2}F1 also stabilizes REH2.
499 That is, the induced downregulation of ^{H2}F1 caused fragmentation of REH2 (4), and we showed here
500 that the converse upregulation of ^{H2}F1 increased the REH2 level *in vivo*. ^{H2}F1 may require most of its
501 zinc fingers to stabilize REH2 because loss of the core structure or positive charge in individual
502 fingers compromised this function. It is feasible that the stabilizing effect of ^{H2}F1 involves substantial
503 changes in the helicase conformation and coordination of its zinc fingers. Notably, all examined ^{H2}F1
504 substitution-mutants were able to associate with REH2, GAP1, and REL1. This suggested that the
505 basic fold or positive charge of the fingers is not essential for the ^{H2}F1 association with other editing
506 components. However, N- or C-terminal truncation of nearly half the size of ^{H2}F1 hampered its normal
507 interactions with the examined editing components. The ^{H2}F1 ΔN accumulated in enriched-
508 mitochondrial extracts but the ^{H2}F1 ΔC localization in mitochondria seemed relatively compromised.
509 Additional studies are needed to pinpoint specific determinants for ^{H2}F1 direct binding to REH2 or its
510 RNA-mediated contacts with other components.
511 Besides the REH2•^{H2}F1 system, other DExH/RHA helicase•Znf protein pairs have been
512 characterized (14). In the DXH30•ZAP system in antivirus protection in humans, the antiviral protein
513 ZAP has four Znf motifs that participate in viral RNA recognition (32, 33). All four fingers lie on a
514 positively charged surface in a crystal structure of ZAP (25) and mutation of basic residues in the

515 fingers inhibited the ZAP antiviral function (33). The ZAP studies imply that stabilization of REH2 by
516 ^{H2}F1 could involve a precise topology of its zinc fingers, and that the ^{H2}F1 fingers may participate in
517 RNA binding. Notably, recombinant ZAP is multimeric (25). If ^{H2}F1 dimerizes, a single REH2C RNP
518 would include 16 zinc fingers. The co-purification of tagged and endogenous ^{H2}F1 from RNase-
519 treated extracts imply direct protein contacts between the ^{H2}F1 copies (S7 Fig.). However, analyses
520 of recombinant ^{H2}F1 WT and mutants are necessary to establish the potential of ^{H2}F1 to multimerize
521 and bind RNA, and to define the role of its fingers. The RNA content in pulldowns of the ^{H2}F1 Znf4
522 variant with four R/K>A substitutions suggested minimal changes in association with target RNAs in
523 mitochondria but a significance loss in non-specific contacts with unrelated transcripts. This suggests
524 that subtle changes in RNA affinity are more likely to affect weak non-specific RNA contacts. The
525 general loss of transcripts examined in the pulldowns of the tested ^{H2}F1 fragments also suggests that
526 efficient RNA association by the REH2C complex *in vivo* involves a full array of zinc fingers in ^{H2}F1.
527 We note that the transcripts examined may associate with either ^{H2}F1, REH2 or both proteins in the
528 native REH2C RNP.
529

530 **REH2 may function as an RNA helicase in kinetoplastid RNA editing**
531
532 Prior studies suggested that REH2 is a functional helicase in RNA editing. REH2 pulldowns
533 from GAP1-depleted extracts exhibit RNA unwinding activity (4), and the mutation of catalytic
534 residues in the predicted RecA1 domain inhibits the unwinding activity in pulldowns of REH2 (23).
535 We have now established that the isolated full-length recombinant REH2 (240 kda) is a *bona fide*
536 RNA helicase enzyme. This further indicates that REH2, the only DExH/RHA helicase in kinetoplastid
537 holo-editosomes provides an ATP-dependent unwinding activity in RNA editing. Additional studies
538 are needed to determine if ^{H2}F1 affects the activity of REH2. Besides REH2, the editing apparatus
539 also requires the DEAD-box RNA helicase REH1 (12, 13). REH1 is not part of the RNPs studied here
540 and seems to lack a direct binding partner. A transient RNA-mediate interaction of REH1 with

541 other editing proteins has been detected (23, 34). REH1 and REH2 are functionally different.
542 REH2 is needed for editing within single blocks, including the first "initiating" block (3). In
543 contrast, REH1 is needed for editing of two or more blocks (i.e., by overlapping gRNAs) but has
544 no effect on the first block, suggesting a role in gRNA exchange (13). Both RNA helicases may
545 promote critical remodeling of RNA or RNP structure. Our ongoing RNA-seq analyses may
546 provide additional functional insights concerning REH2C (Kumar et al., unpublished).
547

548 **Possible roles of editing complex variants**
549
550 The editing apparatus much like the splicing and transcription molecular machines may
551 exhibit dynamic phases of assembly and function. The RECC enzyme has multiple isoforms that
552 include several RNase III (RIII)-like protein subunits. These RIII proteins have the potential to
553 form a large number of binary combinatorial that could modulate substrate recognition (35-37).
554 Also, natural GRBC and REMC isoforms and genetically-induced changes in their protein/RNA
555 organization are emerging. A recurring theme is the variable interaction between the essential
556 GAP1/2 heterotetramer in all editing involving GRBC-bound gRNAs, and MRB3010 (GRBC6)
557 that participates in early editing (1, 6, 38). A controlled interaction of the GAP1/2 tetramer with
558 MRB3010 may modulate editing. For example, GRBC variants in pulldowns of MRB3010 or
559 REH2 differ in relative content of MRB3010 and editing level in associated mRNAs (3, 5).
560 However, RNAi of REH2 or ^{H2}F1 caused a reduced editing in mRNAs in the MRB3010 pulldowns
561 (3, 4). REH2 and ^{H2}F1 features, including those examined here, may affect specific steps in the
562 editing mechanism and we are currently addressing this.
563

564 # Materials and methods
565
566 **Cell Culture**
567

568 *T. brucei* Lister strain 427 29-13 procyclic was grown axenically in log phase in SDM79
569 medium (39) and harvested at a cell density of 1–3x10^7 cells/mL. All transgenic cell lines were
570 induced with tetracycline at 1µg/mL. The REH2 WT-TAP and ^{H2}F1 RNAi cell lines that were
571 used as controls were generated in our lab (3, 4). We have seen that the TAP tag in REH2,
572 including the WT construct, seems to slow the growth of trypanosomes after several days of
573 culture (23). This and presumably incomplete cloning after transfection may account for the
574 uneven expression levels in extracts from independent subcultures. To partially control for this
575 issue, most plasmid constructs used to generate the current data figures were made to use
576 puromycin selection. Most transfections used tetracycline-screened HyClone Fetal Bovine
577 Serum (FBS) (SH30070.03T; GE Healthcare. This enabled a faster cell recovery after
578 transfection than with constructs using phleomycin selection that were originally used in cell
579 lines that also appeared somewhat less stable during subculture. Regardless of this issue,
580 independent analyses of protein associations were consistent with either puromycin or
581 phleomycin constructs.
582

583 **DNA constructs**
584
585 All overexpression and RNAi studies used inducible plasmid constructs. The constructs
586 for ^{H2}F1 RNAi and the REH2 dsRBD2 mutant K1078A/A1086D were previously reported (3, 4).
587 N-terminal deletion constructs for REH2 (ΔN and ΔNds) and ^{H2}F1 (ΔN) were prepared using the
588 In-Fusion® HD Cloning Kit (639648; Clontech). Two PCR amplicons were prepared in each
589 case using CloneAmp™ HiFi PCR Premix (638500; Clontech) and were then gel-eluted using
590 NucleoSpin® Gel and PCR Clean-up (740609.10; Clontech). One amplicon encodes the first 34
591 amino acids of REH2 (primers: F-1503, R-1522), including the predicted REH2 mitochondrial
592 leader sequence (REH2-MLS) (23), that was used for all N-deletion constructs. The other
593 amplicon included the remaining relevant gene fragment sequence: 3070-6501 bases (REH2

594 ΔN), 3280-6501 bases (REH2 ΔNds), or 766-1572 bases (^{H2}F1 ΔN). Three-piece in-fusion
595 reactions were performed to join the two amplicons and pLEW79-ada-TAP plasmid linearized at
596 *XhoI* and *BamHI* (40). The PCR primers (S1 Table) included 5' and 3' terminal homology (15
597 bases) to enable the recombination-based fusion between the amplicons and the plasmid DNA.
598 The REH2 (ΔAOB and ΔOB) and ^{H2}F1 ΔC deletion constructs are also recombination-based
599 fusions of the amplified relevant gene fragment with linearized plasmid DNA. The REH2
600 constructs R2023A, H1998E, R1999E and H1998E/R1999E, and the ^{H2}F1 construct Znf5 C>A
601 were created by site-directed mutagenesis in inverse-PCR reactions of the pLEW79-ada-TAP
602 WT plasmid as the template. pLEW79-ada-TAP was modified from the original pLEW79-TAP
603 (40, 41). The resulting linearized mutant constructs were circularized using the In-Fusion HD
604 Cloning Kit. Other ^{H2}F1 constructs used synthetic gBlock gene fragments (IDT) with mutations.
605 N-terminal fragments of ^{H2}F1 (Znf1, Znf2 and Znf3 R/K>A single finger mutants) replaced the
606 corresponding sequence in the ^{H2}F1 WT construct after digestion with *XhoI* and the internal
607 *ApaI* site in ^{H2}F1. A C-terminal fragment of ^{H2}F1 to generate Znf4R/K>A or Znf5 R/K>A replaced
608 a corresponding sequence in the ^{H2}F1 WT construct after digestion with *ApaI* and *BamH1*. The
609 ^{H2}F1 WT construct was made by ligation of an amplicon with the full open reading frame into
610 pLEW79-ada-TAP plasmid linearized at *XhoI* and *BamHI.* All constructs were confirmed by DNA
611 sequencing, linearized with *NotI*, and transfected in trypanosomes (39).
612

613 **Western Blots and Radioactivity Assays**
614
615 Western blots of REH2, ^{H2}F1 and ^{H2}F2 (subunits of REH2C), GAP1 (alias GRBC2;
616 subunit of GRBC) and A2 (alias MP42; subunit of RECC) were performed as reported (4, 23).
617 Western blots of the GAP1/GAP2 (alias GRBC2/GRBC1) paralogs simultaneously, and of
618 MRB8170 and MRB6070 (subunits of REMC and MRB6070/1590 assemblies, respectively),
619 were performed as previously described (42, 43). GAP1 alone was examined in the main data

620 figures. Both GAP1/GAP2 were examined in S1 and S5 figures. Peroxidase Anti-peroxidase
621 antibody (P1291; Sigma) diluted to 1:200 (v/v) was used to detect the TAP-tag. EF-1 α1
622 antibody (sc-21758; Santa Cruz Biot) diluted to 1:200 (v/v) was used as a cytosolic marker.
623 Protein quantitative analyses using Amersham ECL™ western blot detection reagents were
624 performed in an Amersham Imager 600. RNA ligases in the RECC enzyme were radiolabeled
625 by self-adenylation directly on the beads in IgG pulldowns (44). Unwinding assays of REH2
626 used reported conditions with a few modifications (4) and full-length recombinant His-REH2.
627 The dsRNA substrate in these assays used an A6 mRNA/gRNA pair (23). The A6 pair mimics
628 the endogenous ATPase subunit 6 substrate. The gRNA was transcribed with RNA T7
629 polymerase from an amplicon (S1 Table) after *DraI* restriction digestion and gel purification of
630 the product. The 61-nt gRNA was 5'-labelled with γ^{32}P-ATP using T4 Polynucleotide kinase. The
631 62-nt mRNA was synthetic (IDT). A mix with 3 pmoles of labelled gRNA and 15 pmoles of
632 mRNA was heated at 95° C for 3 min, and then immediately incubated for 30 min at room
633 temperature in the annealing buffer (10 mM MOPS pH 6.5, 1 mM EDTA, and 50 mM KCl). The
634 annealed RNA hybrids were isolated from native 12% PAGE run at 4 ˚C at 50 V for 120 min in
635 0.5x Tris-borate-EDTA buffer. Standard 10 μL reaction mixtures in unwinding buffer (40 mM
636 Tris-Cl pH 8.0, 0.5 mM $MgCl^2$, 0.01% Nonidet P-40, and 2 mM DTT) were incubated for 30 min
637 at 19 °C with 20 cps of hybrid (~20 fmoles) and 3 µg of recombinant REH2 (~12 pmoles).
638 Variations to the standard assay including in the concentration of REH2 or the reaction time are
639 indicated in the text. All assays contained 100 fmoles of unlabeled gRNA as competitor to
640 prevent re-annealing of unwound γ^{32}P-gRNA. The assays were stopped with an equal volume of
641 2x helicase reaction stop buffer (50 mM EDTA, 1% SDS, 0.1% bromophenol blue, 0.1% xylene
642 cyanol, and 20% glycerol) and kept on ice for 5 min. The assays in Fig. 6B were also treated
643 with 0.4U of proteinase K (P8107S; NEB), 25 mM EDTA and 0.5% SDS at 22° C for 30 min.

644 The entire reaction was loaded onto a native 12% PAGE and resolved at 25 V for 120 min at
645 4°C.
646

647 **Cell extracts and purification of protein and RNA from IgG pulldowns**
648
649 Whole cell extracts as well as mitochondria-enriched (mini-mito) extracts were used in
650 this study. Whole-cell extracts were generated by incubation of cell pellets in MRB-Triton buffer
651 (25 mM Tris-Cl pH 8.0, 10 mM MgOAC, 1 mM EDTA, 10 mM KCl, 5% glycerol, 0.5% Triton X-
652 100) at 4 °C for 45 minutes followed by centrifugation at 15,000g for 30 minutes. Mitochondria-
653 enriched extracts were prepared using a simplified protocol similar to others reported earlier (2,
654 45). Namely, cell pellets were resuspended into hypotonic DTE buffer (1 mM Tris-HCl pH 8.0, 1
655 mM EDTA pH 8.0) supplemented with protease inhibitors and disrupted in a Dounce
656 homogenizer. The suspension was passed through a 26-gauge needle as originally described
657 (46). The enriched mitochondrial vesicles were spun down and the cytosolic content in the
658 supernatant discarded. This step improved the recovery of intact REH2 compared to whole-cell
659 extracts. REH2 is more prone to fragmentation than other proteins examined in this study. The
660 following steps were also as in (46). The pellet was resuspended into STM buffer (0.25M
661 Sucrose, 20 mM Tris-HCl pH 8.0, 2 mM $MgCl_2$) supplemented with DNase I, RNase-free
662 (EN0523; Fisher Scientific). The reaction was stopped with one volume of STE buffer (0.25 M
663 Sucrose, 20 mM Tris-HCl pH 8.0, 2 mM EDTA pH 8.0). The enriched mitochondria were spun
664 down and washed in STE buffer. The pellet was resuspended into MRB-Triton buffer and
665 incubated in ice for 15 min. The suspension was spun down at 15,000g at 4 °C for 30 min. The
666 supernatant was collected and stored at -80 °C. In IgG pulldowns of the extracts, ectopically
667 expressed TAP-REH2 and TAP-^{H2}F1 were recovered as reported (4, 23) with some
668 modifications. Approximately 2 mg of protein was mixed with 1x SUPERase·In™ RNase
669 inhibitor (Invitrogen™) and incubated with Dynabeads IgG (11203D; Invitrogen™). The beads

670 were washed five times with 1ml of wash buffer (150 mM NaCl, 1 mM EDTA, 10 mM MgAOc,
671 0.1% NP-40, and 25 mM Tris pH 8.0). Protein was eluted from the beads with 15 μL of 1x SDS
672 loading buffer at 95 °C for 2 min. RNA was extracted by treating the beads with 4U proteinase K
673 (NEB) for 2 hrs at 55 °C, followed by phenol extraction and ethanol precipitation. For some
674 pulldowns, RNase A/T1 mix (EN0551; Fisher Scientific) was applied at 20 U/mg of protein both
675 in the input extract and again while bound to the beads.
676

677 **Quantitative RT-PCR**
678
679 Isolated RNA from the pulldowns or directly from input extracts was treated with DNase
680 I, RNase-free (EN0523; Thermo Scientific™) prior to cDNA synthesis with the iScript™ Reverse
681 Transcription Supermix (Bio-Rad) as described elsewhere (5). The amplifications mixtures (10
682 µl) used SsoAdvanced™ Universal SYBR® Green Supermix (Bio-Rad) and reported
683 oligonucleotides for unedited mRNAs, fully edited mRNA, and reference transcripts (47). Diluted
684 samples of the examined cDNA produced a single amplicon during linear amplification under
685 our conditions. The end-point amplicons described here have been gel-isolated, cloned and
686 confirmed by sequencing as previously described (5). Fold-enrichment of mitochondrial and
687 cytosolic transcripts in IgG pulldowns of tagged proteins (induced extracts), relative to a mock
688 pulldown (uninduced extract), was calculated as follows: Fold = $2^{[-ddCq]}$, where ddCq = Cq test
689 IP – Cq mock IP, as in (5). The relative value for each mutant construct was adjusted to the
690 amount of recovered tagged protein, and subsequently normalized to the tagged WT construct
691 (= 1). The plot in Fig. 5B was constructed using data from 3 independent biological replicate
692 experiments, including a total of six amplicons per data point (i.e., two technical replicate
693 amplicons per assay). Two of the independent experiments (including cultures +/- Tet for each
694 mutant) were performed concurrently. The third independent experiment (one set of cultures per
695 mutant +/- Tet) was conducted on a subsequent date. The replicate experiments showed a

696 consistent sample loading in the assays used in our plots. The examined mutant constructs
697 differed in the amount of non-specific association with Tubulin and other cytosolic transcripts
698 that are normally used as internal reference in antibody pulldowns using a common protein bait.
699 The raw Cq values of examined editing transcripts in the pulldowns and the plotted values after
700 normalization indicated a substantial loss of these transcripts in the truncated mutants.
701 qRT-PCR assays of input extract in S8 Fig. were normalized using the following equation: Ratio
702 (reference/target) = $2^{[Cq(ref) - Cq(target)]}$. This scores the relative difference between the reference
703 and target Cq values. The current plots of input extract used 18S rRNA as reference (S8 Fig.).
704 We obtained similar results with any of these cytosolic transcripts used as a reference: tubulin,
705 1400 or 1390 (Tb927.10.1400 or Tb927.10.1390, respectively).
706

707 **Homology modeling and bioinformatics analysis**
708
709 The multiple-sequence alignment of REH2 and MLE, and that of the ^{H2}F1 zinc finger
710 domains, was done with Clustal Omega (48). Formatting of the fingers alignment was done with
711 BOXSHADE version 3.21 (http:/www.ch.embnet.org/software/BOX_form.html). Sequence
712 alignment of Prp43p, REH2, and other helicases was done using the CDD tool in NCBI (49).
713 The structure-based searches of *T. brucei* REH2 used the program Phyre2 (20). The homology
714 model of REH2 derived from the structure of yeast Prp43p. The inset is a closer view of R2023 and the
715 surround region in the OB-fold. The molecular surface is colored by residue conservation. The image was
716 made using PyMOL version 2.2.
717

718 **Recombinant protein**
719
720 6xHis-REH2 (amino acid residues 30-2167) was amplified by PCR (S1 Table). The gel-
721 purified product was cloned into the NcoI and BamHI sites in the expression vector pET15b by
722 using the NEBuilder® HiFi DNA Assembly Master Mix (E262, NEB) and the appropriate primers.
723 The ligation reaction mixtures were transformed into chemically competent Omnimax cells from

724 ThermoFisher Scientific. Colonies with the correct insert were identified by single-colony PCR
725 and then amplified for plasmid purification. The sequence of the flanking vector region and the
726 insert was checked by DNA sequencing. The plasmid DNA was transformed into Rosetta2 DE3
727 cells (Novagen Inc.) and overexpressed in 4 L of Terrific Broth media by supplementing 2% (v/v)
728 ethanol and 2 mM $MgCl_2$ at 37 °C. Protein induction with 0.5 mM IPTG was done at a OD_{600} of
729 0.8, and the expression was continued for 22 hours at 16 °C. The cell pellet was stored at -80
730 °C overnight and was resuspended in lysis buffer (5 mL/g of cell pellet) of 50 mM Tris-HCl pH
731 8.0, 250 mM NaCl, 1 mM EDTA, and 1 mM DTT along with 10 µg of RNase-free DNase and 15
732 mg of hen egg white lysozyme. The cells were lysed in an Emulsiflex hydraulic press. The cell
733 debris was pelleted at 39,200 x g for 30 minutes at 4 °C. The supernatant with 6xHis-REH2 was
734 batch attached to equilibrated Qiagen Ni-NTA Agarose at 4 °C for 16 hrs. The helicase was
735 eluted with 50 mM Tris-HCl pH 8.0, 300 mM NaCl, 1 mM DDT, and 250 mM imidazole. The first
736 elution of the purification was dialyzed into unwinding assay buffer. This material was tested for
737 the presence of the recombinant protein in 6% SDS-PAGE stained with Commassie blue,
738 western blots and antibody pulldowns, and for activity in dsRNA unwinding activity assays *in*
739 *vitro*.
740

741 # Acknowledgements
742

743 We thank the Read lab for their gift of antibodies against GAP1, TbRGG2 (alias RGG2),
744 MRB6070, MRB8170, and ^{H2}F2. The Afasizhev lab kindly provided antibodies that react against
745 the GAP1/GAP2 paralogs (alias GRBC2/GRBC1) simultaneously. We also thank the Stuart lab
746 for providing the antibodies against A2 (alias MP42). Amna Mushtaq provided detailed
747 comments on the manuscript. Jana Gomez, Elizabeth Alvarez and Melissa Yang helped with
748 the preparation of figures.

References

1. Cruz-Reyes J, Mooers BHM, Doharey PK, Meehan J, Gulati S. Dynamic RNA holoeditosomes with subcomplex variants: Insights into the control of trypanosome editing. WIREs RNA. 2018;e1502.
2. Koslowsky DJ, Sun Y, Hindenach J, Theisen T, Lucas J. The insect-phase gRNA transcriptome in Trypanosoma brucei. Nucleic acids research. 2013.
3. Madina BR, Kumar V, Mooers BH, Cruz-Reyes J. Native Variants of the MRB1 Complex Exhibit Specialized Functions in Kinetoplastid RNA Editing. PloS one. 2015;10(4):e0123441.
4. Kumar V, Madina BR, Gulati S, Vashisht AA, Kanyumbu C, Pieters B, et al. REH2C Helicase and GRBC Subcomplexes May Base Pair through mRNA and Small Guide RNA in Kinetoplastid Editosomes. J Biol Chem. 2016;291(11):5753-64.
5. Madina BR, Kumar V, Metz R, Mooers BH, Bundschuh R, Cruz-Reyes J. Native mitochondrial RNA-binding complexes in kinetoplastid RNA editing differ in guide RNA composition. RNA. 2014;20(7):1142-52.
6. Aphasizheva I, Zhang L, Wang X, Kaake RM, Huang L, Monti S, et al. RNA binding and core complexes constitute the U-insertion/deletion editosome. Mol Cell Biol. 2014;34(23):4329-42.
7. Huang Z, Faktorova D, Krizova A, Kafkova L, Read LK, Lukes J, et al. Integrity of the core mitochondrial RNA-binding complex 1 is vital for trypanosome RNA editing. RNA. 2015.
8. McAdams NM, Simpson RM, Chen R, Sun Y, Read LK. MRB7260 is essential for productive protein-RNA interactions within the RNA editing substrate binding complex during trypanosome RNA editing. RNA. 2018;24(4):540-56.
9. Simpson RM, Bruno AE, Bard JE, Buck MJ, Read LK. High-throughput sequencing of partially edited trypanosome mRNAs reveals barriers to editing progression and evidence for alternative editing. RNA. 2016;22(5):677-95.
10. Simpson RM, Bruno AE, Chen R, Lott K, Tylec BL, Bard JE, et al. Trypanosome RNA Editing Mediator Complex proteins have distinct functions in gRNA utilization. Nucleic acids research. 2017;45(13):7965-83.
11. Shaw PL, McAdams NM, Hast MA, Ammerman ML, Read LK, Schumacher MA. Structures of the T. brucei kRNA editing factor MRB1590 reveal unique RNA-binding pore motif contained within an ABC-ATPase fold. Nucleic acids research. 2015;43(14):7096-109.
12. Missel A, Souza AE, Norskau G, Goringer HU. Disruption of a gene encoding a novel mitochondrial DEAD-box protein in Trypanosoma brucei affects edited mRNAs. Mol Cell Biol. 1997;17(9):4895-903.
13. Li F, Herrera J, Zhou S, Maslov DA, Simpson L. Trypanosome REH1 is an RNA helicase involved with the 3'-5' polarity of multiple gRNA-guided uridine insertion/deletion RNA editing. Proc Natl Acad Sci U S A. 2011;108(9):3542-7.
14. Cruz-Reyes J, Mooers BH, Abu-Adas Z, Kumar V, Gulati S. DEAH-RHA helicase•Znf cofactor systems in kinetoplastid RNA editing and evolutionarily distant RNA processes. RNA Dis. 2016;3(2):e1336.
15. Jarmoskaite I, Russell R. RNA helicase proteins as chaperones and remodelers. Annu Rev Biochem. 2014;83:697-725.
16. Walbott H, Mouffok S, Capeyrou R, Lebaron S, Humbert O, van Tilbeurgh H, et al. Prp43p contains a processive helicase structural architecture with a specific regulatory domain. EMBO J. 2010;29(13):2194-204.

796 17. Robert-Paganin J, Rety S, Leulliot N. Regulation of DEAH/RHA helicases by G-patch
797 proteins. Biomed Res Int. 2015;2015:931857.
798 18. Prabu JR, Muller M, Thomae AW, Schussler S, Bonneau F, Becker PB, et al. Structure
799 of the RNA Helicase MLE Reveals the Molecular Mechanisms for Uridine Specificity and RNA-
800 ATP Coupling. Mol Cell. 2015;60(3):487-99.
801 19. Dhote V, Sweeney TR, Kim N, Hellen CU, Pestova TV. Roles of individual domains in
802 the function of DHX29, an essential factor required for translation of structured mammalian
803 mRNAs. Proc Natl Acad Sci U S A. 2012;109(46):E3150-9.
804 20. Kelley LA, Mezulis S, Yates CM, Wass MN, Sternberg MJ. The Phyre2 web portal for
805 protein modeling, prediction and analysis. Nat Protoc. 2015;10(6):845-58.
806 21. Cruz-Reyes J. MBHM, Kumar K., Doharey P.K., Meehan J., Chaparro L. Control
807 Mechanisms of the Holo-Editosome in Trypanosomes. In: J C-R, M G, editors. RNA Metabolism
808 in Mitochondria. Nucleic Acids and Molecular Biology. 34: Springer, Cham; 2018.
809 22. Jankowsky E. RNA helicases at work: binding and rearranging. Trends in biochemical
810 sciences. 2011;36(1):19-29.
811 23. Hernandez A, Madina BR, Ro K, Wohlschlegel JA, Willard B, Kinter MT, et al. REH2
812 RNA helicase in kinetoplastid mitochondria: ribonucleoprotein complexes and essential motifs
813 for unwinding and guide RNA (gRNA) binding. J Biol Chem. 2010;285(2):1220-8.
814 24. Segal DJ, Crotty JW, Bhakta MS, Barbas CF, 3rd, Horton NC. Structure of Aart, a
815 designed six-finger zinc finger peptide, bound to DNA. J Mol Biol. 2006;363(2):405-21.
816 25. Chen S, Xu Y, Zhang K, Wang X, Sun J, Gao G, et al. Structure of N-terminal domain of
817 ZAP indicates how a zinc-finger protein recognizes complex RNA. Nat Struct Mol Biol.
818 2012;19(4):430-5.
819 26. Klug A. The discovery of zinc fingers and their development for practical applications in
820 gene regulation and genome manipulation. Q Rev Biophys. 2010;43(1):1-21.
821 27. Seiwert SD, Heidmann S, Stuart K. Direct visualization of uridylate deletion in vitro
822 suggests a mechanism for kinetoplastid RNA editing. Cell. 1996;84(6):831-41.
823 28. Rusche LN, Cruz-Reyes J, Piller KJ, Sollner-Webb B. Purification of a functional
824 enzymatic editing complex from Trypanosoma brucei mitochondria. EMBO J. 1997;16(13):4069-
825 81.
826 29. Izzo A, Regnard C, Morales V, Kremmer E, Becker PB. Structure-function analysis of the
827 RNA helicase maleless. Nucleic acids research. 2008;36(3):950-62.
828 30. Masliah G, Barraud P, Allain FH. RNA recognition by double-stranded RNA binding
829 domains: a matter of shape and sequence. Cell Mol Life Sci. 2013;70(11):1875-95.
830 31. Christian H, Hofele RV, Urlaub H, Ficner R. Insights into the activation of the helicase
831 Prp43 by biochemical studies and structural mass spectrometry. Nucleic acids research.
832 2014;42(2):1162-79.
833 32. Ye P, Liu S, Zhu Y, Chen G, Gao G. DEXH-Box protein DHX30 is required for optimal
834 function of the zinc-finger antiviral protein. Protein & cell. 2010;1(10):956-64.
835 33. Guo X, Carroll JW, Macdonald MR, Goff SP, Gao G. The zinc finger antiviral protein
836 directly binds to specific viral mRNAs through the CCCH zinc finger motifs. J Virol.
837 2004;78(23):12781-7.
838 34. Kruse E, Voigt C, Leeder WM, Goringer HU. RNA helicases involved in U-
839 insertion/deletion-type RNA editing. Biochimica et biophysica acta. 2013;1829(8):835-41.
840 35. Carnes J, Soares CZ, Wickham C, Stuart K. Endonuclease associations with three
841 distinct editosomes in Trypanosoma brucei. J Biol Chem. 2011;286(22):19320-30.
842 36. McDermott SM, Luo J, Carnes J, Ranish JA, Stuart K. The Architecture of Trypanosoma
843 brucei editosomes. Proc Natl Acad Sci U S A. 2016;113(42):E6476-E85.
844 37. Carnes J, McDermott S, Anupama A, Oliver BG, Sather DN, Stuart K. In vivo cleavage
845 specificity of Trypanosoma brucei editosome endonucleases. Nucleic acids research.
846 2017;45(8):4667-86.

847 38. Ammerman ML, Hashimi H, Novotna L, Cicova Z, McEvoy SM, Lukes J, et al. MRB3010
848 is a core component of the MRB1 complex that facilitates an early step of the kinetoplastid RNA
849 editing process. RNA. 2011;17(5):865-77.
850 39. Wirtz E, Leal S, Ochatt C, Cross GA. A tightly regulated inducible expression system for
851 conditional gene knock-outs and dominant-negative genetics in Trypanosoma brucei. Molecular
852 and biochemical parasitology. 1999;99(1):89-101.
853 40. Hernandez A, Panigrahi A, Cifuentes-Rojas C, Sacharidou A, Stuart K, Cruz-Reyes J.
854 Determinants for association and guide RNA-directed endonuclease cleavage by purified RNA
855 editing complexes from Trypanosoma brucei. J Mol Biol. 2008;381(1):35-48.
856 41. Panigrahi AK, Schnaufer A, Ernst NL, Wang B, Carmean N, Salavati R, et al.
857 Identification of novel components of Trypanosoma brucei editosomes. RNA. 2003;9(4):484-92.
858 42. Ammerman ML, Downey KM, Hashimi H, Fisk JC, Tomasello DL, Faktorova D, et al.
859 Architecture of the trypanosome RNA editing accessory complex, MRB1. Nucleic acids
860 research. 2012;40(12):5637-50.
861 43. Weng J, Aphasizheva I, Etheridge RD, Huang L, Wang X, Falick AM, et al. Guide RNA-
862 binding complex from mitochondria of trypanosomatids. Mol Cell. 2008;32(2):198-209.
863 44. Sabatini R, Hajduk SL. RNA ligase and its involvement in guide RNA/mRNA chimera
864 formation. Evidence for a cleavage-ligation mechanism of Trypanosoma brucei mRNA editing. J
865 Biol Chem. 1995;270(13):7233-40.
866 45. Hashimi H, Zikova A, Panigrahi AK, Stuart KD, Lukes J. TbRGG1, an essential protein
867 involved in kinetoplastid RNA metabolism that is associated with a novel multiprotein complex.
868 RNA. 2008;14(5):970-80.
869 46. Harris ME, Hajduk SL. Kinetoplastid RNA editing: in vitro formation of cytochrome b
870 gRNA-mRNA chimeras from synthetic substrate RNAs. Cell. 1992;68(6):1091-9.
871 47. Carnes J, Stuart KD. Uridine insertion/deletion editing activities. Methods in enzymology.
872 2007;424:25-54.
873 48. Sievers F, Higgins DG. Clustal Omega, accurate alignment of very large numbers of
874 sequences. Methods Mol Biol. 2014;1079:105-16.
875 49. Marchler-Bauer A, Derbyshire MK, Gonzales NR, Lu S, Chitsaz F, Geer LY, et al. CDD:
876 NCBI's conserved domain database. Nucleic acids research. 2015;43(Database issue):D222-6.
877

878

879 Supporting information

880

881 **S1 Figure. Western blot analyses of RESC associated proteins in antibody pulldowns of**

882 **REH2 and MRB3010**. Immunoprecipitations (IP) from extract with specific antibodies against

883 REH2, MRB3010 or CoxI (mock). **(A)** Western blot analyses examined for the presence of

884 REH2, MRB8170 and MRB6070 proteins. These are markers of REH2C, REMC and a

885 MRB6070/MRB1590-containing subcomplex that associates with RESC, respectively. Extract

886 (Ext) used in the IPs and size markers in kDa (M) are indicated. **(B)** Western blot analyses as in

887 A examining REH2, the GAP1/GAP2 paralogs, and MRB6070. We note that proteins in the IPs

888 are often upshifted relative to the control extract lane. The cause of this upshift is unclear to us
889 but it may be a slight effect on the proteins migration due to the presence of IgG in those
890 samples. IgG in the pulldown lanes is indicated.
891
892 **S2 Figure. Western blot analyses of ectopically-expressed TAP constructs in whole-cell**
893 **and enriched-mitochondrial extracts**. Large-truncation constructs were compared in whole-
894 cell (WC) and enriched-mitochondrial (aka Mini-Mito "MM" extract): (A) REH2-ΔN, (B) REH2-
895 ΔNds, (C) ^{H2}F1-ΔN, and (D) ^{H2}F1-ΔN. Western blots of the tag in these constructs (TAP) and the
896 cytosolic marker eEF-1 indicate a partial enrichment of the constructs in the mini-mito extract.
897
898 **S3 Figure. The OB-fold in yeast helicase Prp43p (crystal structure pdb: 2XAU_B) and *T.***
899 ***brucei* REH2**. (A) Sequence alignment of Prp43p, REH2, and other DExH/RHA helicases. The
900 sequences were aligned using the CDD tool in NCBI. The residue R1979 in REH2 is not
901 conserved in the aligned sequences but the basic amino acid at position 2023 in REH2 (K704 in
902 Prp43p) is conserved. Secondary structure elements are indicated: α-helix (cylinders) and β-
903 strand (arrows). (B) homology model of R2023 in REH2 using the OB fold in Prp43p as a
904 template.
905
906 **S4 Figure. Multi-sequence alignment of a C-terminal segment in *T. brucei* REH2 and**
907 ***Drosophila* MLE DExH/RHA RNA helicases**. The alignment was generated with Clustal
908 Omega (48). Boxes were inserted manually to improve the match between the MLE and REH2
909 residues. Note that H1032, K1033 and T1034 (in red), which make U-specific contacts in MLE,
910 are aligned with H1998, R1999 and T2000 (in red) in REH2. Predicted α-helix (cylinders) and β-
911 strand (arrows) in REH2 are indicated.
912

913 **S5 Figure. Sedimentation analysis of endogenous editing proteins. (A)** 10-30% glycerol
914 gradients of freshly-made mitochondria-enriched extract from 29:13 procyclic trypanosomes.
915 Catalase and RECC complex were used as 11 S and 20 S markers, respectively (23).
916 Endogenous REH2, ^{H2}F1 and ^{H2}F2, GAP1 (GRBC2), GAP2 (GRBC1), and A2 (MP42) were
917 examined in western blots. All panels in this figure derived from the same extract fractions. The
918 data shown is representative of at least two panels for each protein in biological replicate
919 gradients.
920
921 **S6 Figure. Location of the zinc-finger substitutions examined in this study. (A)** Full ^{H2}F1
922 amino acid sequence including the location of eight C2H2 zinc-finger motifs (Znf1-to-8
923 highlighted in different colors)**. (B)** Zinc-finger motifs starting with the N terminal finger at the
924 top, and the amino acid positions spanning each finger in panel A. The R/K>A substitutions in
925 each finger that were examined in this study are marked by a dot.
926
927 **S7 Figure. RNase-resistant co-purification of tagged-^{H2}F1 and endogenous ^{H2}F1.** Western
928 blots of IgG pulldowns from extracts with or without an RNaseA/T1 mix. All panels in this figure
929 derive from the same blot. The upper blot with the tagged-^{H2}F1 bait was cut below the 75 kDa
930 marker. The middle and lower panels were divided between the 50 kDa and 37 kDa marker.
931 The 34.4 kDa RGG2, a typical subunit of the REMC module in the RESC complex. As expected,
932 the RNA-mediated association of RGG2 decreased with the RNase treatment.
933
934 **S8 Figure. Quantitation of steady-state RNA transcripts in the input mitochondrial**
935 **extracts used in the IgG pulldowns.** Independent biological replicates (two independent
936 cultures used in Fig. 5) with Cq average values and one standard deviation (+/-1SD, *n*=2) were
937 plotted. dCq of steady-state RNA transcripts in lysates relative to background 18s rRNA used as
938 reference [dCq = $2^{(\text{target Cq} - \text{ref Cq})}$]. Shorter bars indicate a smaller differential versus 18s rRNA in

939 the sample. For example, ND7 is relatively abundant compared to other transcripts in the
940 sample (i.e., it has a lower Cq). The WT construct is induced or not (+/-). All mutants are
941 induced. All end-point amplicons were examined in gels to confirm that they were single
942 products during linear amplification. Abbreviation of the RNA names is as in Fig. 5B.

943

944 **S1 Table. DNA oligonucleotides, gBlocks (IDT) and synthetic RNA.**

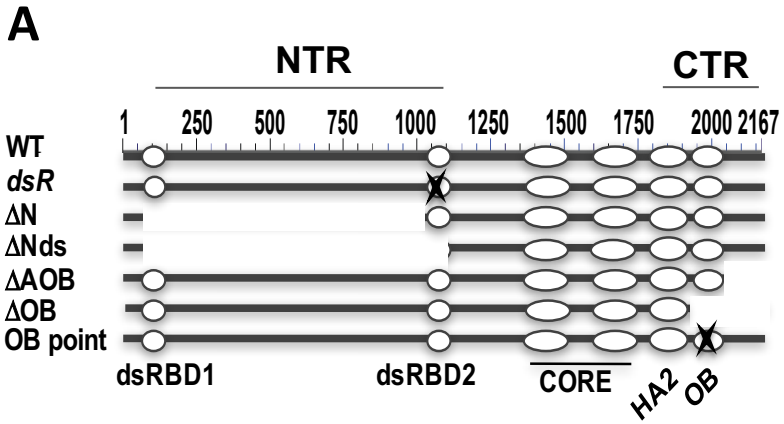

NAME	MUTATION	DOMAINS AFFECTED	MW
dsR	K1078A/A1086D	dsRBD2	242
ΔN	Δ34-1023	dsRBD1	132
ΔNds	Δ34-1093	dsRBD1/dsRBD2	124
ΔAOB	Δ1908-2167		228
ΔOB	Δ2045-2167	OB fold	213
1979	R1979A	OB fold	242
1998	H1998E	OB fold	242
1999	R1999E	OB fold	242
98/99	H1998E/R1999E	OB fold	242
2023	R2023A	OB fold	242

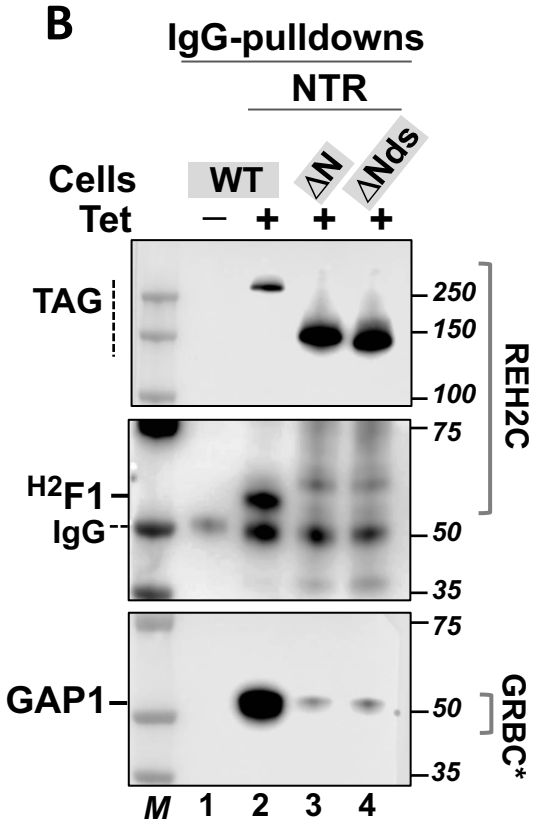

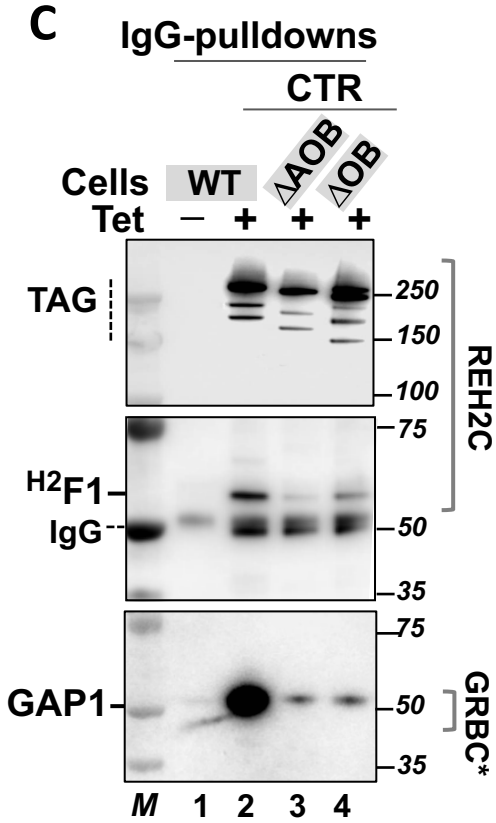

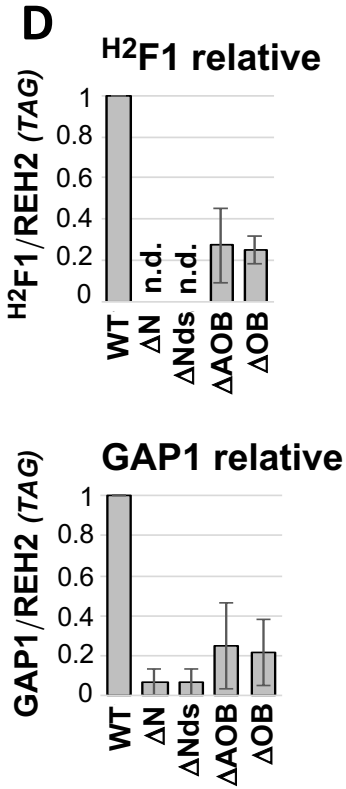

Figure 1

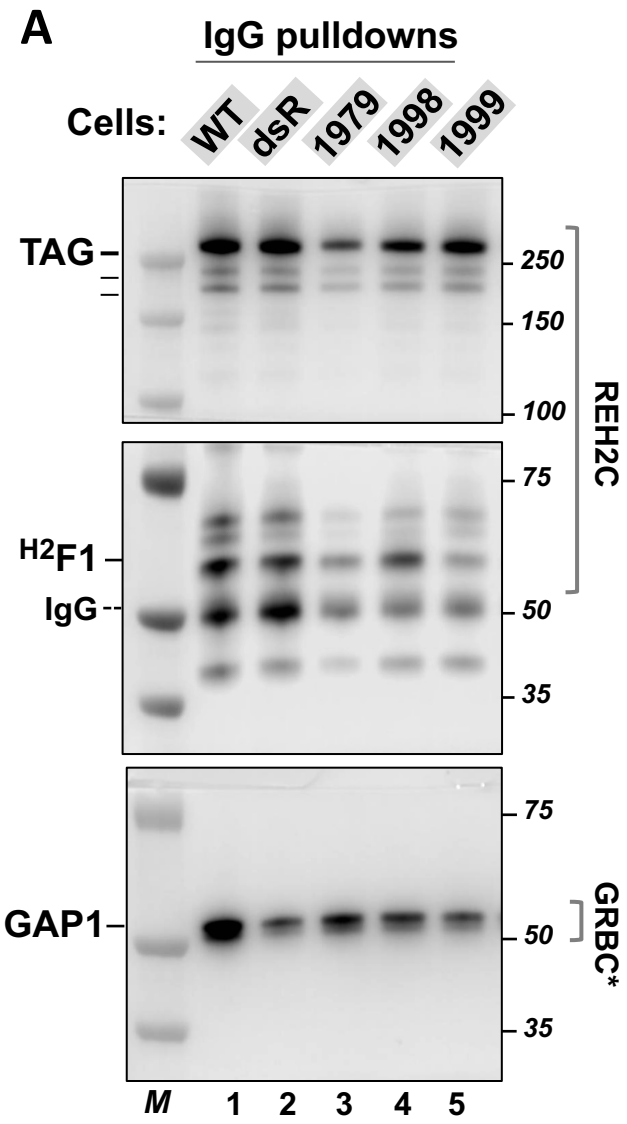
A
IgG pulldowns
Cells:
WT
dsR
1979
1998
1999
TAG
H2F1
IgG
GAP1
250
150
100
75
50
35
REH2C
GRBC*
M
1
2
3
4
5

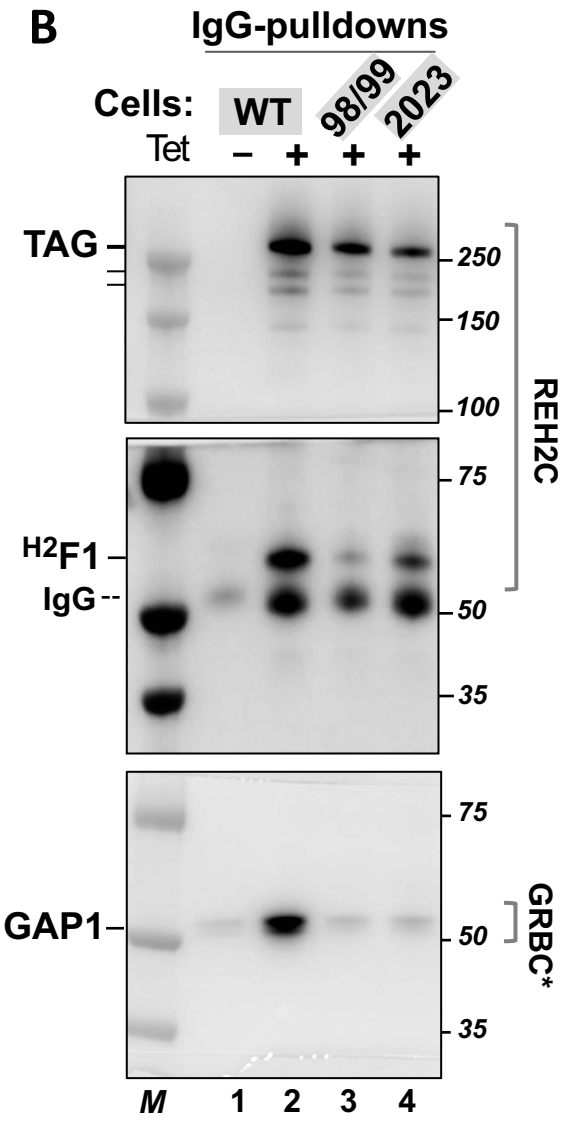
B
IgG-pulldowns
Cells:
WT
98/99
2023
Tet
–
+
+
+
TAG
H2F1
IgG
GAP1
250
150
100
75
50
35
REH2C
GRBC*
M
1
2
3
4

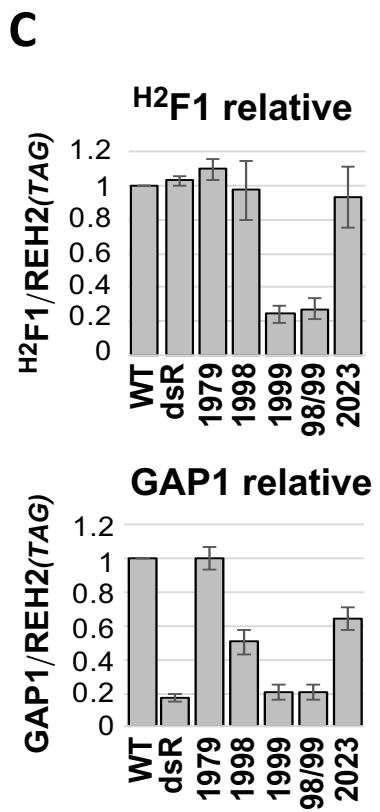
C
H2F1 relative
H2F1/REH2(TAG)
1.2
1
0.8
0.6
0.4
0.2
0
WT
dsR
1979
1998
1999
98/99
2023
GAP1 relative
GAP1/REH2(TAG)

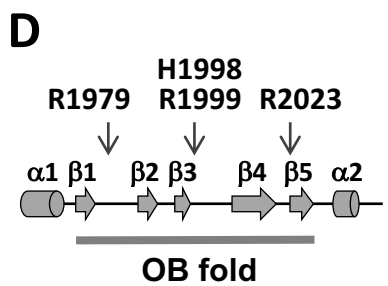
D
R1979
H1998
R1999
R2023
α1
β1
β2
β3
β4
β5
α2
OB fold

Figure 2

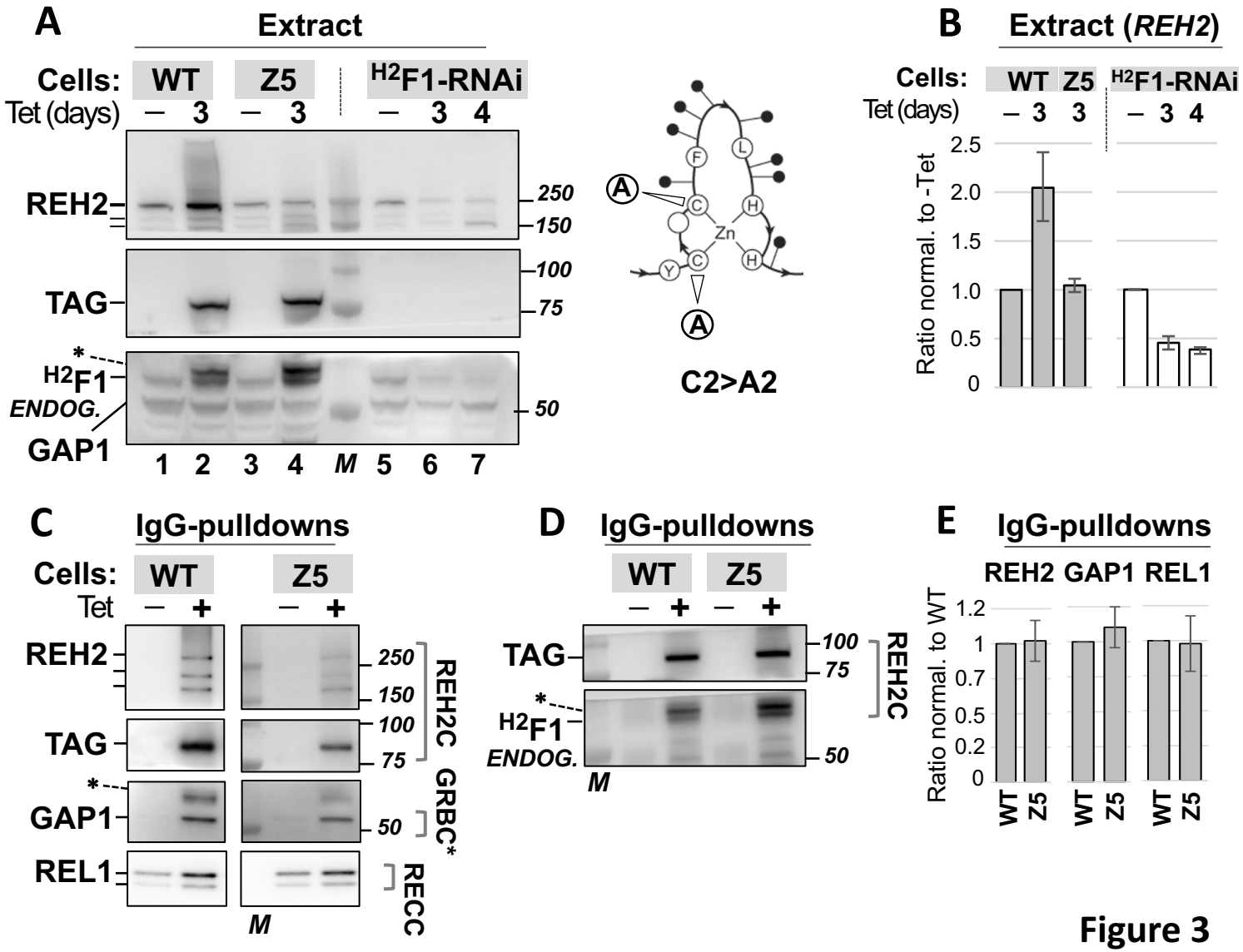
A
Extract
Cells: WT Z5 H2F1-RNAi
Tet (days) – 3 – 3 – 3 4
REH2
TAG
H2F1
ENDOG.
GAP1
250
150
100
75
50
1 2 3 4 M 5 6 7
C2>A2
B
Extract (REH2)
Cells: WT Z5 H2F1-RNAi
Tet (days) – 3 3 – 3 4
Ratio normal. to -Tet
2.5
2.0
1.5
1.0
0.5
0
C
IgG-pulldowns
Cells: WT Z5
Tet – + – +
REH2
TAG
GAP1
REL1
M
REH2C
GRBC*
RECC
D
IgG-pulldowns
WT Z5
– + – +
TAG
H2F1
ENDOG.
M
REH2C
E
IgG-pulldowns
REH2 GAP1 REL1
Ratio normal. to WT
1.2
1
0.7
0.5
0.2
0
WT Z5 WT Z5 WT Z5

Figure 3

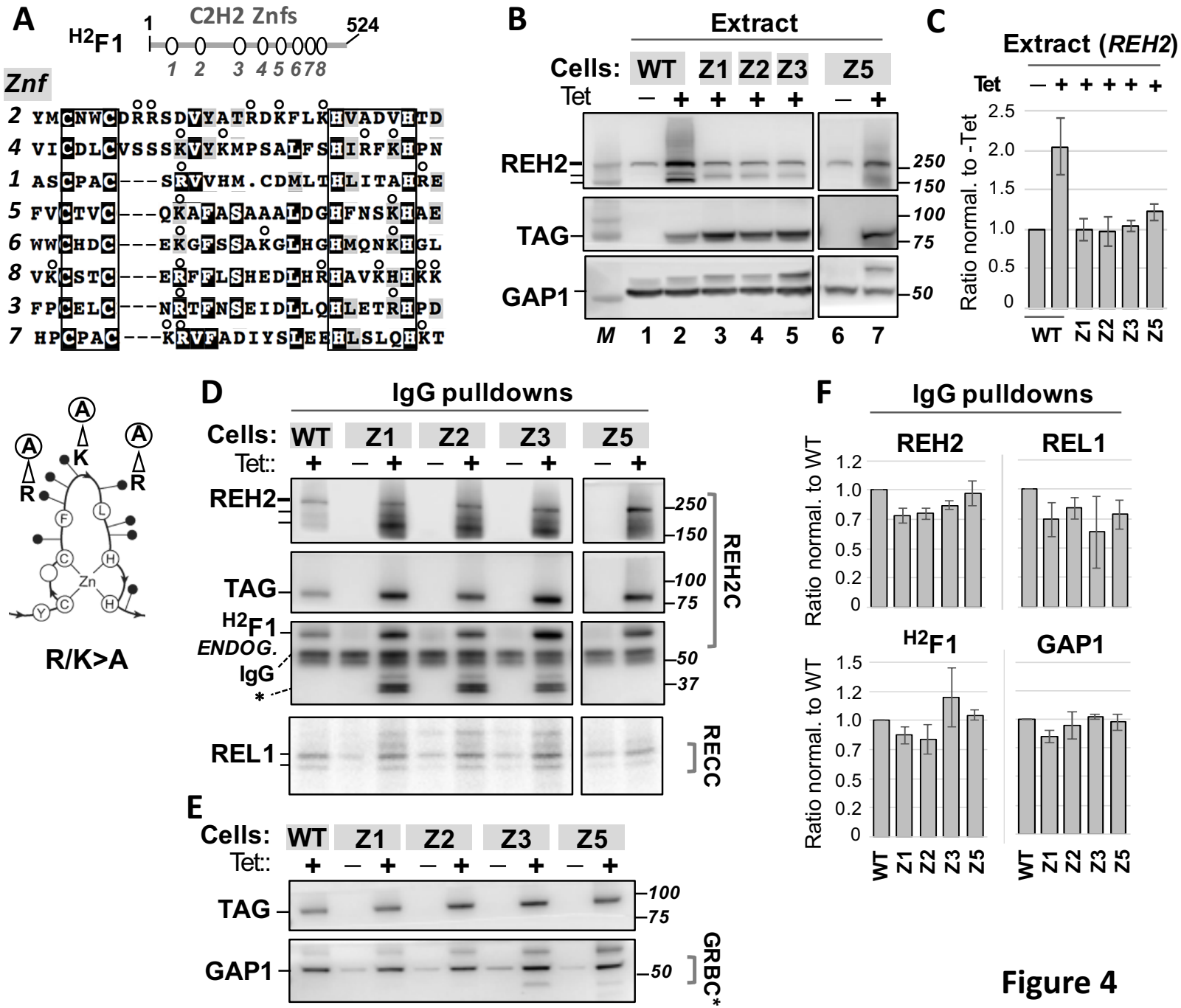
A
H2F1
C2H2 Znfs
1
524
1 2 3 4 5 6 7 8
Znf
2 YMCNWCDRRSDVYATRDKFLKHVADVHTD
4 VICDLCVSSSKVYKMPSALFSHIRFKHPN
1 ASCPAC---SRVVHM.CDMLTHLITAHRE
5 FVCTVC---QKAFASAAALDGHFNSKHAE
6 WWCHDC---EKGFSSAKGLHGHMQNKHGL
8 VKCSTC---ERFFLSHEDLHRHAVKHHKK
3 FPCELC---NRTFNSEIDLLQHLETRHPD
7 HPCPAC---KRVFADIYSLEEHLSLQHKT
B
Extract
Cells: WT Z1 Z2 Z3 Z5
Tet – + + + + – +
REH2
TAG
GAP1
250
150
100
75
50
M 1 2 3 4 5 6 7
C
Extract (REH2)
Tet – + + + + +
Ratio normal. to -Tet
2.5
2.0
1.5
1.0
0.5
0
WT Z1 Z2 Z3 Z5
A
K
R
R
F
L
C
H
Zn
Y
C
H
R/K>A
D
IgG pulldowns
Cells: WT Z1 Z2 Z3 Z5
Tet:: + – + – + – + – +
REH2
TAG
H2F1
ENDOG.
IgG
*
REL1
250
150
100
75
50
37
REH2C
RECC
E
Cells: WT Z1 Z2 Z3 Z5
Tet:: + – + – + – + – +
TAG
GAP1
100
75
50
GRBC*
F
IgG pulldowns
REH2
REL1
H2F1
GAP1
Ratio normal. to WT
1.2
1.0
0.7
0.5
0.2
0
1.5
WT Z1 Z2 Z3 Z5

Figure 4

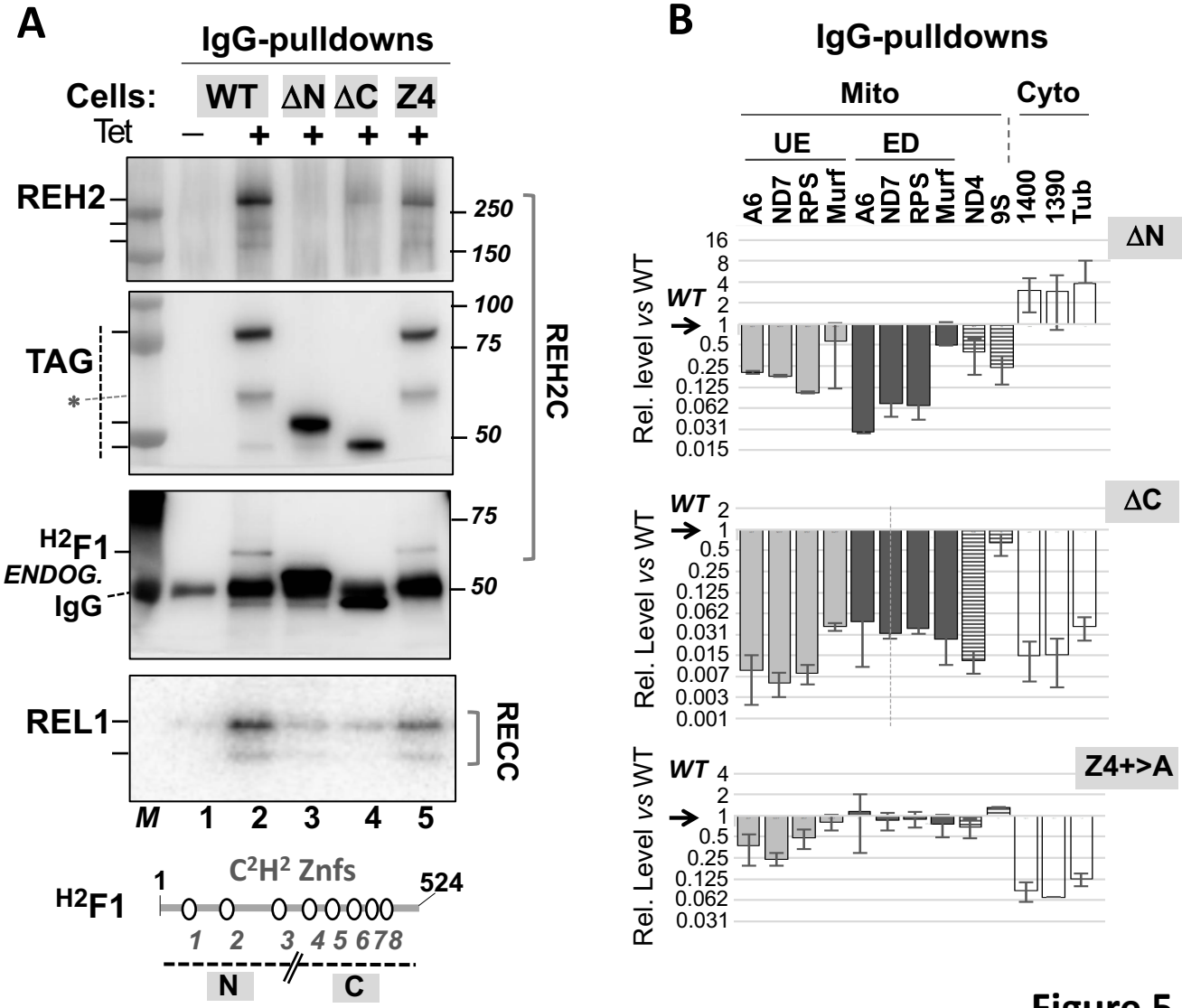
A
IgG-pulldowns
Cells:
WT
ΔN
ΔC
Z4
Tet
REH2
TAG
H2F1
ENDOG.
IgG
REL1
250
150
100
75
50
REH2C
RECC
M
1
2
3
4
5
C2H2 Znfs
524
N
C
B
Mito
Cyto
UE
ED
A6
ND7
RPS
Murf
ND4
9S
1400
1390
Tub
Rel. level vs WT
Rel. Level vs WT
WT
Z4+>A

Figure 5

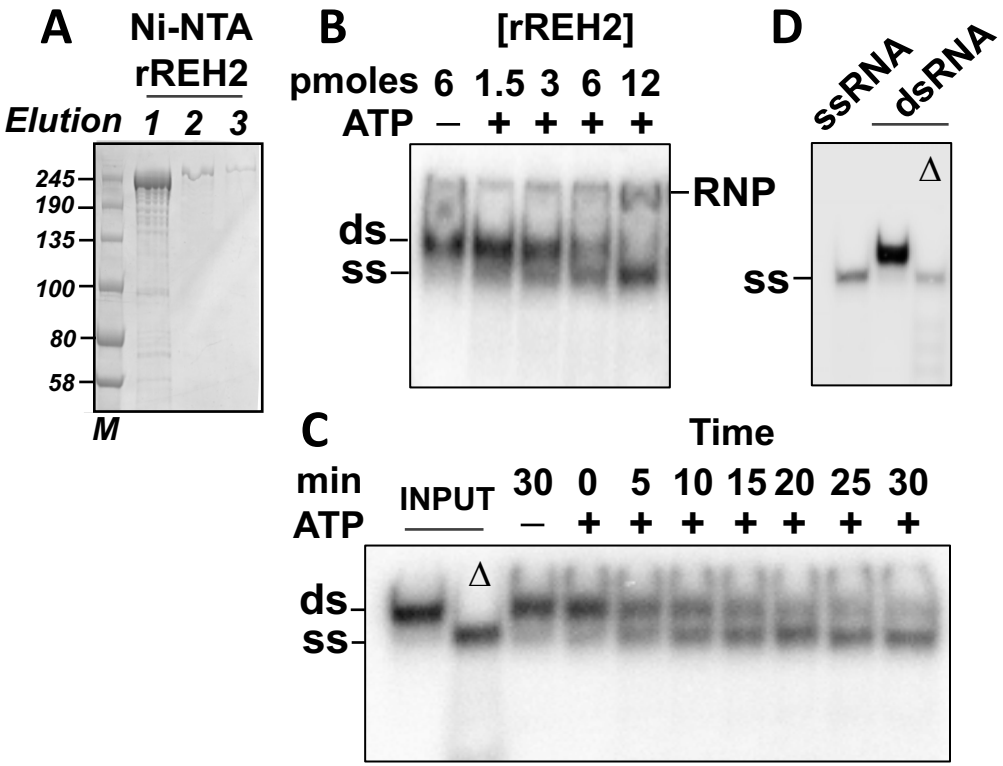
A
Ni-NTA
rREH2
Elution 1 2 3
245
190
135
100
80
58
M
B
[rREH2]
pmoles 6 1.5 3 6 12
ATP – + + + +
RNP
ds
ss
D
ssRNA
dsRNA
Δ
ss
C
Time
min INPUT 30 0 5 10 15 20 25 30
ATP – + + + + + + +
Δ
ds
ss

Figure 6